

**Erratum: The evolution of circular, non-equatorial orbits of Kerr black holes due to gravitational-wave emission**  
[Phys. Rev. D 61, 084004 (2000)]

Scott A. Hughes

PACS numbers: 04.30.Db, 04.30.-w, 04.25.Nx, 95.30.Sf

Equation (4.52) of this paper should read

$$Z_{l-m-k}^{H,\infty} = (-1)^{l+k} \bar{Z}_{lmk}^{H,\infty} .$$

As a consequence, the odd  $l$  contributions to the gravitational waveforms shown are off by a minus sign. However, all of the rates of change discussed in this paper ( $\dot{E}$ ,  $\dot{L}_z$ ,  $\dot{Q}$ ,  $\dot{r}$ ,  $\dot{i}$ ) are unchanged since they only depend on the square of this coefficient.

arXiv:gr-qc/9910091v3 5 Jan 2001

# The evolution of circular, non-equatorial orbits of Kerr black holes due to gravitational-wave emission

Scott A. Hughes

*Theoretical Astrophysics, California Institute of Technology, Pasadena, CA 91125*  
*Department of Physics, University of Illinois at Urbana-Champaign, Urbana, IL 61801*

A major focus of much current research in gravitation theory is on understanding how radiation reaction drives the evolution of a binary system, particularly in the extreme mass ratio limit. Such research is of direct relevance to gravitational-wave sources for space-based detectors (such as LISA). We present here a study of the radiative evolution of circular (*i.e.*, constant Boyer-Lindquist coordinate radius), non-equatorial Kerr black hole orbits. Recent theorems have shown that, at least in an adiabatic evolution, such orbits evolve from one circular configuration into another, changing only their radius and inclination angle. This constrains the system's evolution in such a way that the change in its Carter constant can be deduced from knowledge of gravitational wave fluxes propagating to infinity and down the black hole's horizon. Thus, in this particular case, a local radiation reaction force is not needed. In accordance with post-Newtonian weak-field predictions, we find that inclined orbits radiatively evolve to larger inclination angles (although the post-Newtonian prediction overestimates the rate of this evolution in the strong field by a factor  $\lesssim 3$ ). We also find that the gravitational waveforms emitted by these orbits are rather complicated, particularly when the hole is rapidly spinning, as the radiation is influenced by many harmonics of the orbital frequencies.

PACS numbers: 04.30.Db, 04.30.-w, 04.25.Nx, 95.30.Sf

## I. INTRODUCTION

### A. Motivation: the relativistic two-body problem in the extreme mass ratio limit

An outstanding problem in general relativity is the evolution of binary systems with strong gravity and compact bodies. Although post-Newtonian approximations very successfully describe the evolution of such binaries when the bodies are widely separated [1], no approximation schemes work well when the bodies are close: in general, there is no small parameter that can be used to develop any approximations. Numerical relativity will be needed to accurately evolve and understand the dynamics of compact binaries in the strong-field regime. Despite much effort and progress [2], numerical relativity is still several years away from being able to solve the most interesting strong-field problems such as the final inspiral and merger of binary black hole and binary neutron star systems. The full relativistic two-body problem is thus likely to remain unsolved into the near future.

There is one limit in which the two-body problem can be solved to very high accuracy with tools available now: the limit in which the mass of one body,  $m_1 \equiv \mu$ , is much less than the mass of the other, a black hole with  $m_2 \equiv M$ . The body of mass  $\mu$  can be treated as perturbing the “background” black hole spacetime generated by the mass  $M$ . The evolution of the system can then be studied with perturbation techniques such as the Teukolsky equation [3].

This limit is in fact of great interest since extreme mass ratio systems (*e.g.*, a compact body of mass  $1 - 10 M_\odot$  orbiting a black hole of mass  $10^{5-7} M_\odot$ ) are among the most important candidate sources for space-based gravitational-wave detectors such as the Laser Interferometer Space Antenna (LISA) [4]. Recent estimates place the number of such extreme mass ratio inspirals, occurring at distances  $D \lesssim 1$  Gpc, in the range of 1/year to 1/month [5,6]. LISA should be able to measure the gravitational waves emitted by these inspirals with amplitude signal-to-noise ratios around  $10 - 100$  [7].

During its last year of inspiral, the compact body orbits in the very strong-field region near the massive black hole's event horizon, typically spiraling due to gravitational-wave emission from  $r \lesssim 10M$  to the innermost stable circular orbit. (We use units with  $G = c = 1$ .) The orbit is dynamically unstable there, so the body quickly plunges into the hole, cutting off the signal. During this year, the system emits roughly  $10^5$  gravitational-wave cycles, mostly in LISA's most sensitive frequency band (depending upon the mass of the black hole). If it is possible to accurately track the waves' phase during this year (using, for instance, the technique of matched filtering with templates), it will be possible to make very accurate measurements of the black hole's characteristics, and perhaps to make detailed tests of general relativity (for example, by “mapping” the massive object's spacetime to test whether it is in fact a black hole or a more exotic compact object [8]).

arXiv:gr-qc/9910091v3 5 Jan 2001

Making such accurate measurements will require a high-precision means of modeling gravitational waves from extreme mass ratio binaries. One can divide in two the influences which drive such systems' evolutions: the radiation reaction force (backreaction due to gravitational-wave emission causing the orbiting body to lose orbital energy and spiral in), and environmental influences (effects due to the systems' astrophysical environment). It is possible that environmental influences for the most important sources will be negligible. Perhaps the most important influence is the interaction of the orbiting body with material accreting onto the massive black hole: black holes in the target mass range  $10^{5-7}M_{\odot}$  reside at the core of galaxies where they accrete gas from their environment. In the majority of cases, accretion occurs at rather low rates (several orders of magnitude less than the Eddington rate [10]). For these "normal" galaxies, much evidence [9,10] suggests that the gas accretes via an advection dominated accretion flow (ADAF). Narayan has shown that the influence of an ADAF upon an inspiraling compact body will be far less important than radiation reaction [10]: the timescale for ADAF drag to change an orbit's characteristics is many orders of magnitude longer than the radiation reaction timescale. If accretion drag remains the most important environmental influence on extreme mass ratio binaries, then radiation reaction is likely to be the only important element needed to construct precise models of their evolution. Because in general we expect orbits to be inclined and rather eccentric [6], techniques must be constructed for analyzing the radiative evolution of generic Kerr orbits.

If the mass ratio is extreme, one can use a linear approximation to study the system's evolution. Split the spacetime metric into a "background" black hole piece plus a perturbation:  $g_{\alpha\beta} = g_{\alpha\beta}^{\text{Kerr}}(M, a) + h_{\alpha\beta}(\mu)$ . The system's evolution is governed by the properties of the full spacetime  $g_{\alpha\beta}$ , but it is convenient to regard the motion of the small body  $dx^{\mu}/d\tau$  as a geodesic of  $g_{\alpha\beta}^{\text{Kerr}}$  plus corrections from an instantaneous radiation reaction force  $f_{\text{RR}}^{\mu}(\tau)$ :

$$\frac{dx^{\mu}}{d\tau} = \left. \frac{dx^{\mu}}{d\tau} \right|_{\text{geodesic}} + \int f_{\text{RR}}^{\mu}(\tau) d\tau . \quad (1.1)$$

The force  $f_{\text{RR}}^{\mu}(\tau)$  (where  $\tau$  is proper time measured by the orbiting body) encapsulates the manner in which the motion of the body deviates from motion in the background spacetime. In particular, it embodies the effects of radiation reaction, causing the inspiral of the small body toward the black hole as the system's orbital energy and angular momentum are bled off by gravitational-wave emission. Detailed quantitative understanding of this force is needed to precisely model the evolution of extreme mass ratio binaries.

There currently exists a well-defined prescription for calculating the radiation reaction force. Quinn and Wald [11] and Mino *et al.* [12] have independently and by several different techniques derived a rather general expression for the force, depending upon a "tail" which is integrated over the past worldline of the orbiting body's motion. This tail reflects the fact that, because of scatter from spacetime curvature, the domain of dependence of radiation for an event lies inside the light cone. Various groups are currently working on implementations of the force (see, *e.g.*, Refs. [13,14] for approaches based on direct evaluation of the Quinn-Wald-Mino quantities on the worldline, and [15–18] for an approach based on multipole decomposition). It is likely to be some time before practical implementations for astrophysically realistic cases will be available.

## B. Radiation reaction without radiation reaction forces

One can parameterize Kerr orbits by their three constants of motion: energy  $E$ ,  $z$ -component of angular momentum  $L_z$ , and Carter constant  $Q = p_{\theta}^2 + \cos^2\theta [a^2(1 - E^2) + \csc^2\theta L_z^2]$  [19]. A given set  $(E, L_z, Q)$  can be thought of as a point in the space of all possible Kerr orbits. When orbits evolve due to radiation reaction, they generate a trajectory  $[E(t), L_z(t), Q(t)]$  through this space. One can then regard the major goal of radiation reaction research as understanding all physically allowed trajectories through this orbital phase space.

Consider the limit in which the system's evolution is adiabatic: the timescale  $\tau_{\text{RR}}$  for the orbit's parameters to change is much longer than an orbital period  $T$ . In this limit, the system spends many periods near any point on its phase space trajectory: each point on the trajectory is itself very nearly a geodesic orbit. [If the evolution is not adiabatic, the system moves along this trajectory too rapidly for this to be the case: it does not remain near any set of constants  $(E, L_z, Q)$  long enough to approximate an orbit.] One can then regard the system as slowly passing from one geodesic configuration to another.

The mechanism pushing the system from one geodesic to the next is a radiation reaction force. In this limit, the effect of this force can be understood as a slow change to the "constants" of the orbital motion. Might it not be possible to *indirectly* infer the change in these constants and thereby deduce the radiative evolution without actually computing the radiation reaction force? For example, the energy carried by gravitational waves to infinity and down the event horizon is well understood (cf. Refs. [20] and [21]). Might it be possible to deduce from the gravitational-wave flux the change of all three orbital constants and thereby deduce, in the adiabatic limit, the system's radiative evolution?

In general, it is *not* possible to deduce the rate at which all three constants so change: the energy and the angular momentum can be read from the gravitational-wave flux, but usually the Carter constant cannot be. This is because the energy and angular momentum are scalars which are linearly constructed from an orbit’s momentum  $p^\mu$ , whereas the Carter constant is a scalar which is quadratically constructed from the momentum.

Consider a particle orbiting a Kerr black hole. At some instant, the particle has momentum  $p_B^\mu$ . This particle radiates for some time and falls into a new orbit with instantaneous momentum  $p_A^\mu$ . The change in the particle’s momentum is  $\delta p^\mu = p_A^\mu - p_B^\mu$ .

The Kerr metric admits a timelike Killing vector  $T_\mu$ , an azimuthal Killing vector  $\Phi_\mu$ , and a Killing tensor  $Q_{\mu\nu}$  (see [22] for an explicit representation of this tensor in Boyer-Lindquist coordinates). The energy of the orbiting particle is given by  $E = -T_\mu p^\mu$ . Thus, the particle has energy  $E_B = -T_\mu p_B^\mu$  before it radiates, and energy  $E_A = -T_\mu p_A^\mu$  after it radiates. The change in the energy is carried away by the radiation:

$$\delta E = E_B - E_A = -T_\mu(p_B^\mu - p_A^\mu) = T_\mu \delta p^\mu . \quad (1.2)$$

If we consider a “graviton limit”<sup>1</sup> of the emitted radiation, then  $\delta p_{\text{graviton}}^\mu = -\delta p^\mu$  is the 4-momentum carried by the radiation itself. The quantity  $\delta E$  is the energy that observers at infinity measure the radiation to carry (or, that it adds to the black hole’s mass after it falls down the event horizon). Since  $\delta E = -T_\mu \delta p_{\text{graviton}}^\mu$  depends only on properties of the gravitons radiated to infinity or down the horizon, one can deduce that the particle’s energy is changed from  $E_B$  to  $E_B - \delta E = E_A$  directly out of the gravitational-wave flux. Using  $\Phi_\mu$  rather than  $T_\mu$ , we see that the change in the particle’s ( $z$ -component of) angular momentum can also be read from the flux.

Consider now the particle’s Carter constant. It is related to the particle’s instantaneous momentum via the Killing tensor:  $Q = Q_{\mu\nu} p^\mu p^\nu$ . Thus, before radiating, the particle has  $Q_B = Q_{\mu\nu} p_B^\mu p_B^\nu$ , and after has  $Q_A = Q_{\mu\nu} p_A^\mu p_A^\nu$ . Writing  $Q_A$  using  $p_A^\mu = p_B^\mu + \delta p^\mu$ , and then evaluating  $Q_B - Q_A$  yields

$$\delta Q = Q_B - Q_A = 2Q_{\mu\nu} p_B^\mu \delta p^\nu + Q_{\mu\nu} \delta p^\mu \delta p^\nu . \quad (1.3)$$

Because this depends explicitly on the local, instantaneous momentum of the particle, this quantity *cannot* be read from the radiation flux. Indeed, dividing by  $\delta\tau$ , taking the limit  $\delta\tau \rightarrow 0$ , and recognizing that in the limit  $\delta p^\mu / \delta\tau$  is the radiation reaction force  $f_{\text{RR}}^\mu$ , we find that the rate of change of the Carter constant is given by

$$\dot{Q} = 2Q_{\mu\nu} p^\mu f_{\text{RR}}^\nu . \quad (1.4)$$

*In general, the radiation reaction force is needed to compute the rate at which the Carter constant changes even in the adiabatic limit.*

In general, “radiation reaction without radiation reaction forces” does not work. There are, however, special cases where it does work. Consider first equatorial orbits. The Carter constant for equatorial orbits is zero, and, since there is no means by which these orbits can be raised out of the equatorial plane (the Kerr metric is reflection symmetric about its equator),  $Q$  remains zero at all times. Thus, the system’s evolution is entirely given by the two quantities  $\dot{E}$  and  $\dot{L}_z$ . This is not surprising. Equatorial orbits can be described with two parameters: a radial measure  $p$  (such as the semi-latus rectum; see [31]), and an eccentricity  $e$ . Orbital evolution is given by the rates at which these parameters change. Connecting the evolution of these two orbital quantities to the evolution of the two “conserved” quantities  $E$  and  $L_z$  fully specifies the system’s evolution. Thus, equatorial orbit evolution can be fixed by examining radiation flux. In particular, since Schwarzschild black holes have no preferred orientation, any Schwarzschild orbit is equatorial and can be evolved by studying radiation flux. Detailed studies of such orbits’ evolution (and the waveforms they produce) can be found in [28–32].

Kerr black holes have a preferred orientation defined by their spin axis, so equatorial and non-equatorial orbits are quite different. Various evolutionary studies of such orbits have been done: see [33] for a first analysis of waveforms and energy fluxes from circular equatorial orbits; [34] for a study of waveforms and energy fluxes from eccentric equatorial orbits; [35] for an analysis of the stability of circular equatorial orbits; and [7] for an examination of circular equatorial orbits with an emphasis on measurability by LISA.

Circular, non-equatorial Kerr orbits can also be analyzed without radiation reaction forces. (“Circular orbit” means “orbit of constant Boyer-Lindquist coordinate radius”). The properties of such orbits in the limit  $a = M$  are discussed

---

<sup>1</sup>For the purposes of this illustrative calculation, it is far simpler to regard the radiation as a stream of particles for which we can identify an associated 4-momentum. In the limit in which the radiation is clearly wavelike, we must be far more careful to make sure that we confine our analysis to the wave zone, and to average over several wavelengths. A more careful analysis in this limit would likely modify Eqs. (1.3) and (1.4).

at length in [36].) Such an orbit has non-zero Carter constant, but it turns out that, in the adiabatic limit, its evolution is entirely determined by the radiated energy and angular momentum. This is because, as has recently been proved [37–39], circular orbits remain circular as they adiabatically evolve due to radiation reaction. That is, to very high accuracy the system evolves from one circular configuration to another. By requiring that the circularity condition hold at all times, we can write down a relationship  $\dot{Q} = \dot{Q}(\dot{E}, \dot{L}_z)$  [cf. Eq. (3.5)]. Thus, measurement of the fluxes  $\dot{E}$  and  $\dot{L}_z$  is enough to entirely specify the evolution of the system. This is not surprising: inclined circular systems can be described by two parameters, a radius  $r$  and an inclination angle  $\iota$ . Despite the fact that such orbits have three non-trivial conserved quantities, one would guess that information about the evolution of two of these quantities should suffice to specify the system’s evolution.

The remainder of this paper discusses the evolution of inclined, circular orbits of Kerr black holes. A first analysis of such evolution was given by Shibata [40] before the “circular goes to circular” theorems were proved. Noting that in the  $a = 0$  limit the Carter constant contains information about the  $x$  and  $y$  components of the angular momentum, Shibata argues that even in the case  $a \neq 0$  the evolution of  $Q$  should be driven by  $L_x$  and  $L_y$  carried in gravitational radiation [41]. Neglecting certain terms since their evolutionary timescales will be much longer than other terms, Shibata gives an expression for Carter constant evolution in terms of quantities that can be measured in the radiation flux. Although we have not checked this explicitly, we suspect that Shibata’s prescription is adequate for describing how  $Q$  changes in the weak field [where the timescale separation he describes should be quite accurate, and also where radiation flux down the horizon is unimportant (see [41])], but would not work well in the strong field.

### C. The Sasaki-Nakamura-Teukolsky formalism

The formalism used in this paper to compute waveforms and fluxes is based on the Teukolsky equation [Eq. (4.2)]. The Teukolsky equation describes the (linearized) evolution of perturbations to the Kerr spacetime. In particular, it gives the evolution of the complex Weyl curvature scalar  $\psi_4 = -C_{\alpha\beta\gamma\delta}n^\alpha\bar{m}^\beta n^\gamma\bar{m}^\delta$  (where  $C_{\alpha\beta\gamma\delta}$  is the Weyl curvature tensor and  $n^\alpha, \bar{m}^\beta$  are legs of the Newman-Penrose null tetrad; see, *e.g.*, [22]). All information about the radiation flux at infinity and down the horizon can be extracted from  $\psi_4$ .

The Teukolsky equation has a source term which depends on an integral over the world line of the orbiting particle. In this paper, we work in the frequency domain, thus requiring a Fourier transform of this source. For this Fourier transform to be formally valid, we must know the full worldline from  $t = -\infty$  to  $\infty$ . Since, in fact, we do not yet know the radiative corrections, we approximate the worldline as a Kerr geodesic orbit. This approximation is valid in the adiabatic limit, and is in fact how the assumption of adiabatic motion mathematically manifests itself: we use the zeroth order, geodesic motion to find the first order radiative correction.

For each set of constants  $(E, L_z, Q)$  there is in fact an entire family of orbits. Each member of the family is distinguished by the particle’s initial position at the beginning of a period. In constructing the source function, we assume that all of these orbits are equivalent in the sense that they generate the same radiative trajectory through  $(E, L_z, Q)$  parameter space. This should be a valid assumption in the adiabatic limit. To see this, pick a parameter space trajectory with some initial conditions, and divide it into segments of length  $T$  (a single period). In the adiabatic limit, each segment has identical constants, but has different initial conditions and so corresponds to a different member of the orbital family. Over many periods, the orbiting particle averages all members of the family. Thus, in the adiabatic limit, the initial conditions of the trajectory make no difference: if we had chosen different initial conditions, the orbiting particle would have sampled all members of the family anyway. This averaging lets us assume that we may pick one representative member of the orbital family and obtain reliable results.

To actually solve the Teukolsky equation, we integrate its source over a Green’s function constructed from the equation’s homogeneous solutions. Here, we run into a well-known technical difficulty: because it has a long-ranged potential, the asymptotic forms of these homogeneous solutions are somewhat ill-behaved. In a numerical computation, we need to be able to calculate the Teukolsky solution at some field point  $r$  by integrating from an asymptotic regime where its behavior is simple. Because of the long-ranged potential, it is very difficult to properly set the phase of the asymptotic solution: as  $r \rightarrow \infty$ , it has an outgoing piece  $\propto e^{i\omega r^*}$  whose amplitude grows at a rate  $r^4$  times an ingoing piece  $\propto e^{-i\omega r^*}$  [ $r^*$  is the Kerr “tortoise coordinate”, cf. Eq. (4.6)]. The ingoing piece is completely lost in a numerical calculation.

To get around this problem, we use the Sasaki-Nakamura equation, Eq. (4.19). Solutions of the Sasaki-Nakamura equation are related to solutions of the Teukolsky equation by a simple transformation [Eq. (4.24)]; and, since the Sasaki-Nakamura equation has a short-ranged potential, its asymptotic solutions are very well-behaved. We thus integrate the Sasaki-Nakamura equation, perform a transformation to the Teukolsky solution, use that solution to construct a Green’s function, and then integrate the Green’s function over the Teukolsky source. From this final integration, we construct the Weyl scalar  $\psi_4$  and obtain all needed details about the radiation flux.

## D. Overview and organization of this paper

Throughout this paper, an overdot denotes  $d/dt$  and a prime denotes  $d/dr$ . An overbar denotes complex conjugation. Unless otherwise specified,  $t$ ,  $r$ ,  $\theta$ , and  $\phi$  refer to the Boyer-Lindquist coordinates. The superscript “rad” refers to a quantity carried by radiation. Hence,  $\dot{E}^{\text{rad}}$  is the flux of energy carried by radiation. By contrast,  $\dot{E}$  is the change rate of an orbit’s energy. We assume that  $\dot{E} + \dot{E}^{\text{rad}} = 0 = \dot{L}_z + \dot{L}_z^{\text{rad}}$ .

Section II gives an overview of the properties of circular Kerr geodesic orbits. We review the equations governing these geodesics, and then review the properties of equatorial orbits in Sec. II A. In Sec. II B we discuss non-equatorial orbits, giving relations that  $E$ ,  $L_z$ ,  $Q$ , and the radius  $r$  must satisfy for the orbit to be circular. Frequencies of motion for non-equatorial orbits are calculated in Sec. II C. There are two important frequencies for circular, non-equatorial orbits: an azimuthal frequency  $\Omega_\phi$  (connected to the time for an orbiting particle to pass through its range of  $\phi$ ), and a polar frequency  $\Omega_\theta$  (related to the time for an orbiting particle to pass through its range of  $\theta$ ). These frequencies are equal when  $a = 0$ , and approach one another in the weak-field limit. In the strong field, and particularly for rapidly spinning black holes, they can be quite different.

In Sec. III, we begin analyzing the effects of radiation reaction. By requiring that circular orbits remain circular as the system evolves, we derive in Sec. III A an expression relating  $\dot{Q}$  and  $\dot{r}$  to  $\dot{E}$  and  $\dot{L}_z$ . We show in Sec. III B that requiring the system to evolve adiabatically strongly constrains the applicability of this analysis to astrophysical systems. For orbits in the strong field, the analyses of this paper can only be considered valid if the mass ratio of the system is quite extreme [cf. Eq. (3.16)].

In Sec. IV, we describe in detail the Sasaki-Nakamura-Teukolsky formalism used to compute all radiation reaction quantities. Although this formalism has been used by several other authors in the past, we have found that the literature contains several critical errors (particularly for non-zero black hole spin). Thus, we discuss this formalism in some detail (hopefully without introducing any errors of our own). Section IV A reviews the Teukolsky equation [3], discussing the asymptotic behavior of its homogeneous solutions, using those solutions to construct a Green’s function, and then using the Green’s function to construct  $\psi_4$  and extract the waveforms and fluxes. (Extended discussion of the separated  $\theta$  dependence and efficient algorithms for computing that dependence are given in Appendix A.) In Sec. IV B, we introduce the Sasaki-Nakamura transformation and equation, and show how one can obtain the homogeneous Teukolsky solutions from the well-behaved Sasaki-Nakamura solution. In Sec. IV C, we develop the source term of the Teukolsky equation, and use it in Sec. IV D to complete the description of  $\psi_4$ .

Section V describes the numerical implementation used in this study. In Sec. V A we sketch the code used to compute all radiation reaction quantities. We describe in Sec. V B several tests (“sanity checks”) that this code was required to pass: in the weak field, the code was required to reproduce results that are well known from previous post-Newtonian analyses; and, in the strong-field Schwarzschild limit, radiation reaction quantities for inclined orbits were checked to see that they obeyed a simple relation to quantities computed for the equatorial plane. (In addition, many quantities were spot-checked against results for equatorial orbits that were kindly provided by D. Kennefick and L. S. Finn; they agreed in all cases.)

Results for strong-field Kerr orbits are given in Sec. VI. We discuss the waveforms and energy fluxes for a few representative orbits in Sec. VI A. We find that as the black hole’s spin increases, the effect of high harmonics of the orbit’s fundamental frequencies becomes more important. Mathematically, this is due to the fact that the transmissivity of the Teukolsky potential to radiation increases as the spin parameter  $a$  is dialed up. More physically, it is probably due to the fact that for large spins and strong-fields, the frequencies  $\Omega_\phi$  and  $\Omega_\theta$  become quite different, and so the motion of the source becomes almost aperiodic. The orbital motion, which is the source of the radiation, thus requires many harmonics of these frequencies to be accurately described. In Sec. VI B we describe a radiation reaction sequence for strong-field orbits near a black hole with spin parameter  $a = 0.8M$ . We examine a set of many orbits, parameterized by the radius  $r$  and inclination angle  $\iota$ . At each parameter space point  $(r, \iota)$ , we compute the direction  $(\dot{r}, \dot{\iota})$  in which radiation reaction drives the system. These directions would be the tangent vectors to the trajectories  $[r(t), \iota(t)]$  that evolving circular orbits would follow as they evolved. An interesting result is that the change in inclination angle  $\iota$  found in the strong field is rather smaller (by a factor  $\lesssim 3$ ) than what one would predict based on extrapolating post-Newtonian theory.

The spin choice  $a = 0.8M$  is a reasonable value for a black hole whose angular momentum has been buffered by magnetohydrodynamic extraction of spin energy, such as are described by some models of quasar engines [23,24]. In general, whenever a black hole is coupled to an accretion disk by magnetic fields, one expects there to be a buffering torque that can significantly impact the hole’s spin [25]. However, if the hole’s evolution is driven by thin-disk accretion (particularly by photon capture in the thin-disk limit as described in [26]), or the hole is produced by the merger of two black holes (such as a result of galaxy collisions), the spin can be much larger:  $a = 0.998M$  is the prediction of photon-buffered thin-disk accretion. An analysis of radiation reaction on circular orbits in this large spin regime will be presented in a separate paper [27].

Some concluding discussion is given in Sec. VII. In particular, we note that the assumption of adiabaticity might not be reasonable in the real world. This assumption would not be needed if it were possible to compute the instantaneous radiation reaction force  $f_{\text{RR}}^\mu$ . This illustrates the importance of such a force, and provides further impetus to workers implementing the radiation reaction force.

## II. CIRCULAR, GEODESIC KERR ORBITS

In this section, we discuss bound circular orbits of Kerr black holes, without incorporating radiation reaction. Kerr geodesics are governed by the following four equations [19]:

$$\Sigma^2 \left( \frac{dr}{d\tau} \right)^2 = [E(r^2 + a^2) - aL_z]^2 - \Delta [r^2 + (L_z - aE)^2 + Q] \equiv R, \quad (2.1a)$$

$$\Sigma^2 \left( \frac{d\theta}{d\tau} \right)^2 = Q - \cot^2 \theta L_z^2 - a^2 \cos^2 \theta (1 - E^2) \equiv \Theta^2, \quad (2.1b)$$

$$\Sigma \left( \frac{d\phi}{d\tau} \right) = \csc^2 \theta L_z + aE \left( \frac{r^2 + a^2}{\Delta} - 1 \right) - \frac{a^2 L_z}{\Delta}, \quad (2.1c)$$

$$\Sigma \left( \frac{dt}{d\tau} \right) = E \left[ \frac{(r^2 + a^2)^2}{\Delta} - a^2 \sin^2 \theta \right] + aL_z \left( 1 - \frac{r^2 + a^2}{\Delta} \right). \quad (2.1d)$$

The quantities  $E$ ,  $L_z$ , and  $Q$  (“energy”, “ $z$ -component of angular momentum”, and “Carter constant”) specify a family of geodesic orbits. They are conserved along any orbit in this family. Particular members of the family are specified by initial conditions. In Eqs. (2.1a–2.1d),  $\Sigma \equiv r^2 + a^2 \cos^2 \theta$  and  $\Delta = r^2 - 2Mr + a^2$ . Eqs. (2.1a) and (2.1b) have been divided by  $\mu^2$  and Eqs. (2.1c) and (2.1d) by  $\mu$  (where  $\mu$  is the mass of the orbiting particle). Because of this,  $E$ ,  $L_z$ , and  $Q$  as used throughout this paper are the specific energy, angular momentum and Carter constant:  $E = E^{\text{usual}}/\mu$ ,  $L_z = L_z^{\text{usual}}/\mu$ , and  $Q = Q^{\text{usual}}/\mu^2$ .

The right-hand side of Eq. (2.1b) goes to zero as the orbiting particle’s position approaches the turning points of its  $\theta$  motion,  $\theta_{\text{max}}$  and  $\theta_{\text{min}}$ . This causes problems in a numerical implementation [cf. the source term of Sec. IV C, which could be written as an integral over  $(d\theta/dt)^{-1}$ ]. To deal with this problem, we transform to a coordinate that is much better behaved at the turning points. First, define the variable  $z = \cos^2 \theta$ . Equation (2.1b) becomes

$$\begin{aligned} \frac{d\theta}{d\tau} &= \pm \frac{\sqrt{z^2 [a^2(1 - E^2)] - z [Q + L_z^2 + a^2(1 - E^2)] + Q}}{(r^2 + a^2z)\sqrt{1 - z}}, \\ &= \pm \frac{\sqrt{\beta(z_+ - z)(z - z_-)}}{(r^2 + a^2z)\sqrt{1 - z}}. \end{aligned} \quad (2.2)$$

The plus sign corresponds to motion from  $\theta_{\text{min}}$  to  $\theta_{\text{max}}$ , and vice versa for the minus sign. We have defined  $\beta = a^2(1 - E^2)$ , and  $z_\pm$  are the two roots of the quadratic in the top line of Eq. (2.2).

Next, define the variable  $\chi$  via  $z = z_- \cos^2 \chi$ . The parameter  $\chi$  ranges from 0 to  $2\pi$ . As  $\chi$  varies from 0 to  $2\pi$ ,  $\theta$  goes from  $\theta_{\text{min}}$  to  $\theta_{\text{max}}$  (at  $\chi = \pi$ ) then back to  $\theta_{\text{min}}$ . Examining  $dz/d\theta$  and  $dz/d\chi$  we see that

$$\begin{aligned} \frac{d\chi}{d\theta} &= \sqrt{\frac{1 - z}{z_- - z}}, \quad 0 \leq \chi \leq \pi; \\ &= -\sqrt{\frac{1 - z}{z_- - z}}, \quad \pi \leq \chi \leq 2\pi. \end{aligned} \quad (2.3)$$

Combining Eqs. (2.2) and (2.3), we obtain the geodesic equation for  $\chi$ :

$$\frac{d\chi}{d\tau} = \frac{\sqrt{\beta(z_+ - z)}}{r^2 + a^2z}. \quad (2.4)$$

This form is perfectly well behaved over the entire orbit. Although the interest here is in circular orbits, circularity was not assumed at any point in this derivation. Equation (2.4) could be useful in the study of generic Kerr orbits.

We specialize to circular orbits from this point onward. These orbits satisfy  $R = 0 = R'$ . The first condition guarantees that  $dr/d\tau = 0$ , so that the radius does not change. The second states that the orbit is eternally at a turning point of its radial motion. In addition, the condition  $R'' < 0$  must be met for the orbit to be stable.

An orbit can be fixed by specifying  $r$  and  $L_z$ : from the conditions  $R = 0 = R'$ ,  $Q$  and  $E$  are determined. The Carter constant and angular momentum determine the amount by which the orbit is inclined from the equatorial plane. As in [38,44], we will use the following inclination angle:

$$\cos \iota = \frac{L_z}{\sqrt{L_z^2 + Q}}. \quad (2.5)$$

This inclination angle is a constant of the motion and is very easy to compute. One could define other inclination angles [*e.g.*, the arctangent of  $(d\theta/d\tau)/(d\phi/d\tau)$  evaluated at  $\theta = \pi/2$ , the angle at which infinitely distant observers would see the particle cross the equatorial plane]. We shall stick with  $\iota$  as defined above since it is adequate for this analysis.

### A. Equatorial orbits

To begin, consider  $Q = 0$ . By Eq. (2.5) these orbits have  $\iota = 0^\circ$  or  $180^\circ$ , lying in the equatorial plane. By Eq. (2.1b),  $d\theta/d\tau = 0$ , so they remain in the equatorial plane at all times. The conditions  $R = 0 = R'$  yield the following formulae for  $E(r)$  and  $L_z(r)$ :

$$E^{\text{pro}} = \frac{1 - 2v^2 + qv^3}{\sqrt{1 - 3v^2 + 2qv^3}}, \quad (2.6a)$$

$$L_z^{\text{pro}} = rv \frac{1 - 2qv^3 + q^2v^4}{\sqrt{1 - 3v^2 + 2qv^3}}, \quad (2.6b)$$

$$E^{\text{ret}} = \frac{1 - 2v^2 - qv^3}{\sqrt{1 - 3v^2 - 2qv^3}}, \quad (2.6c)$$

$$L_z^{\text{ret}} = -rv \frac{1 + 2qv^3 + q^2v^4}{\sqrt{1 - 3v^2 - 2qv^3}}. \quad (2.6d)$$

Here,  $v \equiv \sqrt{M/r}$  and  $q \equiv a/M$ . The superscripts “pro” and “ret” correspond to prograde and retrograde orbits, respectively<sup>2</sup>.

As seen by observers at infinity, the particle in this equatorial orbit moves with azimuthal frequency

$$\Omega_\phi = \frac{d\phi}{dt} = \frac{d\phi/d\tau}{dt/d\tau} = \pm \frac{M^{1/2}}{r^{3/2} \pm aM^{1/2}}, \quad (2.7)$$

where the upper sign refers to prograde and the lower to retrograde orbits.

### B. Non-equatorial orbits

Non-equatorial orbits have  $Q \neq 0$ . We will use the following algorithm to ensure that we find all stable orbits at some particular radius  $r$ :

1. The most stable orbit is the prograde equatorial orbit, so it makes a useful starting point. Pick a value of  $r$  and use Eqs. (2.6a) and (2.6b) to calculate this orbit’s energy and angular momentum. Since it is equatorial,  $Q = 0$ .
2. Decrease the angular momentum  $L_z$ , holding  $r$  fixed. Solve the system of equations  $R = 0 = R'$  to find  $Q$  and  $E$ . These equations admit simple analytic solutions for  $Q(r, L_z)$  and  $E(r, L_z)$  [Eqs. (2.8) and (2.9)].

---

<sup>2</sup>Throughout this paper, we distinguish between prograde and retrograde orbits by the sign of  $L_z$ . Another common convention is to switch the sign of the black hole’s spin  $a$ . This is not useful here since the characteristics of the orbit should smoothly vary from prograde to retrograde as the orbit’s inclination varies from  $0^\circ$  to  $180^\circ$ .



3. Repeatedly decrement the angular momentum and solve again for  $Q(r, L_z)$  and  $E(r, L_z)$  until either the angular momentum reaches  $L_z^{\text{ret}}$  (indicating that we have reached the least-bound retrograde equatorial orbit) or else  $R'' = 0$ . Orbits with  $R'' = 0$  are marginally bound; orbits with still lower values of  $L_z$  are not stable, and are thus not of interest. Radiation reaction causes such orbits to catastrophically plunge into the black hole.

As mentioned above, when  $r$  and  $L_z$  are specified, the equations  $R = 0 = R'$  admit a simple solution for  $E$  and  $Q$ :

$$E(r, L_z) = \frac{a^2 L_z^2 (r - M) + r \Delta^2}{a L_z M (r^2 - a^2) \pm \Delta \sqrt{r^5 (r - 3M) + a^4 r (r + M) + a^2 r^2 (L_z^2 - 2Mr + 2r^2)}} , \quad (2.8)$$

$$Q(r, L_z) = \frac{[(a^2 + r^2)E(r, L_z) - a L_z]^2}{\Delta} - [r^2 + a^2 E(r, L_z)^2 - 2a E(r, L_z) L_z + L_z^2] . \quad (2.9)$$

There are two roots for  $E$ . Only one of these roots is physical; the other typically gives an energy less than the energy of the most strongly bound orbit (the prograde equatorial orbit). In this paper, we shall focus exclusively on orbits for which the plus sign in the denominator of Eq. (2.8) is physical. The minus sign turns out to be physical only for strong-field orbits of very rapidly rotating holes; an analysis of such orbits will be presented in a separate paper [27]. At any rate, since we have fixed the choice of root in Eq. (2.8), circular orbits are entirely determined by choosing  $r$  and  $L_z$  (and checking that  $R'' \leq 0$ ).

### C. Frequencies of non-equatorial orbits

As the particle orbits, its motions in  $\theta$  and  $\phi$  are separately periodic. The periods for these two motions are generally different. In this section, we derive expressions for the periods  $T_\theta$  and  $T_\phi$ , and show that if we perform our analysis in a certain frame we need only worry about  $T_\theta$ . The analysis here is very similar to that of Wilkins [36], but does not specialize to  $a = M$ .

#### 1. Period of $\theta$ motion

We first calculate the time (as seen by observers at infinity) for the particle to move from  $\chi = 0$  to  $\chi$ . Combining Eqs. (2.1d) and (2.4),

$$\frac{dt}{d\chi} = \frac{\gamma + a^2 E z}{\sqrt{\beta(z_+ - z)}} , \quad (2.10)$$

where

$$\gamma \equiv E \left[ \frac{(r^2 + a^2)^2}{\Delta} - a^2 \right] + a L_z \left( 1 - \frac{r^2 + a^2}{\Delta} \right) . \quad (2.11)$$

The time it takes to go from 0 to  $\chi$  is then

$$\begin{aligned} t_0(\chi) &= \int_0^\chi d\chi' \frac{\gamma + a^2 E z(\chi')}{\sqrt{\beta[z_+ - z(\chi')]}}, \\ &= \frac{\gamma}{\sqrt{\beta z_+}} \left[ K \left( \sqrt{z_- / z_+} \right) - F \left( \pi/2 - \chi, \sqrt{z_- / z_+} \right) \right] \\ &\quad + a^2 E \sqrt{\frac{z_+}{\beta}} \left[ E \left( \pi/2 - \chi, \sqrt{z_- / z_+} \right) - F \left( \pi/2 - \chi, \sqrt{z_- / z_+} \right) - E \left( \sqrt{z_- / z_+} \right) + K \left( \sqrt{z_- / z_+} \right) \right] . \end{aligned} \quad (2.12)$$

On the last line,  $F(\varphi, k)$  is the incomplete elliptic integral of the first kind,  $K(k)$  is the complete elliptic integral of the first kind;  $E(\varphi, k)$  and  $E(k)$  are respectively the incomplete and complete elliptical integrals of the second kind (using the notation of [47]).

Equation (2.12) only applies to the interval  $0 \leq \chi \leq \pi/2$ . It is straightforward to generalize to the interval  $\pi/2 \leq \chi \leq \pi$ :

$$\begin{aligned} t(\chi) &= t_0(\chi) , & 0 \leq \chi \leq \pi/2 , \\ &= t_0(\pi/2) + t_0(\chi - \pi/2) , & \pi/2 \leq \chi \leq \pi . \end{aligned} \quad (2.13)$$

Similar formulae can be written down for  $\pi \leq \chi \leq 2\pi$ ; it turns out that they are not needed. We could add any constant to  $t(\chi)$ ; this would specify a different member of the orbital family corresponding to  $(E, L_z, Q)$ .

The particle moves through one fourth of its  $\theta$  range as  $\chi$  varies from 0 to  $\pi/2$ . Hence,  $T_\theta$ , the period of the particle's  $\theta$  motion, is given by

$$T_\theta = 4t_0(\pi/2) = \frac{4\gamma}{\sqrt{\beta z_+}} K\left(\sqrt{z_-/z_+}\right) + 4a^2 E \sqrt{\frac{z_+}{\beta}} \left[ K\left(\sqrt{z_-/z_+}\right) - E\left(\sqrt{z_-/z_+}\right) \right]. \quad (2.14)$$

The corresponding frequency of  $\theta$  motion is  $2\pi/T_\theta$ .

## 2. Period of $\phi$ motion

In this subsection we calculate the angle  $\phi$  accumulated as the particle moves from 0 to  $\chi$ , and use it to calculate the azimuthal period  $T_\phi$ .

Applying the transformations  $z = \cos^2 \theta = z_- \cos^2 \chi$  to Eq. (2.1c) and combining the result with Eq. (2.4) yields

$$\frac{d\phi}{d\chi} = \frac{1}{\sqrt{\beta(z_+ - z)}} \left( \frac{L_z}{1 - z} + \delta \right), \quad (2.15)$$

where

$$\delta = aE \left( \frac{r^2 + a^2}{\Delta} - 1 \right) - \frac{a^2 L_z}{\Delta}. \quad (2.16)$$

Integrating Eq. (2.15) from 0 to  $\chi$  gives the amount of  $\phi$  accumulated as the particle orbits:

$$\begin{aligned} \phi(\chi) &= \phi_0(\chi), & 0 \leq \chi \leq \pi/2, \\ &= \phi_0(\pi/2) + \phi_0(\chi - \pi/2), & \pi/2 \leq \chi \leq \pi; \end{aligned} \quad (2.17)$$

where

$$\begin{aligned} \phi_0(\chi) &= \frac{1}{\sqrt{\beta z_+}} \left\{ L_z \left[ \Pi\left(\pi/2, -z_-, \sqrt{z_-/z_+}\right) - \Pi\left(\pi/2 - \chi, -z_-, \sqrt{z_-/z_+}\right) \right] \right. \\ &\quad \left. + \delta \left[ K\left(\sqrt{z_-/z_+}\right) - F\left(\pi/2 - \chi, \sqrt{z_-/z_+}\right) \right] \right\}. \end{aligned} \quad (2.18)$$

Here  $\Pi(\varphi, n, k)$  is the incomplete elliptical integral of the third kind, again using the notation of [47]. In a period  $T_\theta$ , the particle moves through an azimuthal angle  $\Phi$  given by

$$\Phi = 4\phi_0(\pi/2) = \frac{4}{\sqrt{\beta z_+}} \left[ L_z \Pi\left(\pi/2, -z_-, \sqrt{z_-/z_+}\right) - \delta K\left(\sqrt{z_-/z_+}\right) \right]. \quad (2.19)$$

Unless  $\Phi$  equals  $2\pi$  (which is only the case for  $a = 0$ ), the periods of  $\theta$  and  $\phi$  motion will be incommensurate. This is potentially problematic, since it is not clear which period is the fundamental one to use for describing the orbits and gravitational radiation. However, as shown by Cutler, Kennefick and Poisson (Sec. IID of [31]), we can expand the  $\phi$  motion in a Fourier series of  $\Omega_\theta$  harmonics:

$$\frac{d\phi}{dt} = \sum_{n=0}^{\infty} a_n e^{in\Omega_\theta t}. \quad (2.20)$$

First, integrate this up to obtain

$$\phi(t) = a_0 t + \sum_{n=1}^{\infty} b_n e^{in\Omega_\theta t}, \quad (2.21)$$

where  $b_n = ia_n/n\Omega_\theta$ . Next, average this over a time  $T_\theta$ . The sum goes to zero by periodicity, so

$$a_0 \equiv \Omega_\phi = \frac{\Phi}{T_\theta} = \frac{\Phi}{2\pi} \Omega_\theta. \quad (2.22)$$

Analyze the system in a coordinate system that is rotating at angular velocity  $\Omega_\phi$ , so that  $\phi' = \phi - \Omega_\phi t$ . In this coordinate system, the only frequency that matters in the analysis of azimuthal motion is  $\Omega_\theta$  (and its harmonics):

$$\phi'(t) = \sum_{n=1}^{\infty} b_n e^{in\Omega_\theta t} . \quad (2.23)$$

Thus  $\Omega_\theta$  and its harmonics are the only frequencies that are needed in order to analyze the motion of the orbiting particle in this coordinate system. The only timescale we need be concerned about is  $T_\theta$ .

### III. RADIATION REACTION: INITIAL CONSIDERATIONS

In this section, we begin to consider radiation reaction and how it modifies the orbits from their purely geodesic form. The requirement that circular orbits remain circular allows us to write down a simple condition for  $\dot{Q}$  and  $\dot{r}$  given  $\dot{E}$  and  $\dot{L}_z$ . This analysis is presented in Sec. III A.

As discussed in the Introduction, we assume that the system evolves in an adiabatic manner: the change in any orbital parameter  $q$  over one period  $T_\theta$  must be much less than  $q$ . By insisting that the evolution be adiabatic everywhere, we derive conditions on the mass ratio  $\mu/M$ . As we show in Sec. III B, this leads to stringent conditions when the particle is near the black hole, but essentially irrelevant conditions when the particle is in the weak field. When discussing astrophysical gravitational-wave sources, our results can be considered relevant only when these conditions are met.

#### A. Circular remains circular

As discussed in Sec. I B, it has recently been shown [37–39] that, under adiabatic radiation reaction, circular orbits evolve from one circular configuration to another (except possibly in the very strong-field regime, as the orbiting particle begins to plunge into the black hole). An orbit which is circular remains circular.

For the orbit to remain circular at all times, the equations  $\dot{R} = 0$  and  $\dot{R}' = 0$  must hold, where

$$\begin{aligned} \dot{R} &= \dot{r}R' + 2E\dot{E}r^4 + \left[2a^2E\dot{E} - 2L_z\dot{L}_z - \dot{Q}\right]r^2 + 2\left[\dot{Q} + 2(\dot{L}_z - a\dot{E})(L_z - aE)\right]Mr - a^2\dot{Q} , \\ \dot{R}' &= \dot{r}R'' + 8E\dot{E}r^3 + 2\left[2a^2E\dot{E} - 2L_z\dot{L}_z - \dot{Q}\right]r + 2\left[\dot{Q} + 2(\dot{L}_z - a\dot{E})(L_z - aE)\right]M . \end{aligned} \quad (3.1)$$

These quantities are found by taking the time derivative of  $R$  and  $R'$  [where  $R$  is defined in Eq. (2.1a)].

Notice that  $\dot{R} = 0$  and  $\dot{R}' = 0$  can be combined into a single matrix equation,

$$A \cdot v_1 + B \cdot v_2 = 0 , \quad (3.2)$$

where

$$\begin{aligned} v_1 &= \begin{pmatrix} \dot{E} \\ \dot{L}_z \end{pmatrix} , \\ v_2 &= \begin{pmatrix} \dot{Q} \\ \dot{r} \end{pmatrix} . \end{aligned} \quad (3.3)$$

The matrices  $A$  and  $B$  can then be explicitly written out by gathering the proper terms in  $\dot{E}$ ,  $\dot{L}_z$ ,  $\dot{Q}$ , and  $\dot{r}$ . The solution for  $\dot{Q}$  and  $\dot{r}$  in terms of  $\dot{E}$  and  $\dot{L}_z$  is now transparent: solving Eq. (3.2) for  $v_2$  yields

$$v_2 = -B^{-1} \cdot A \cdot v_1 \equiv -C \cdot v_1 . \quad (3.4)$$

Thus, we may write

$$\begin{aligned} \dot{Q} &= -\frac{c_{11}}{d}\dot{E} - \frac{c_{12}}{d}\dot{L}_z , \\ \dot{r} &= -\frac{c_{21}}{d}\dot{E} - \frac{c_{22}}{d}\dot{L}_z , \end{aligned} \quad (3.5)$$

where

$$\begin{aligned}
c_{11}(Q, E, L_z, r) \equiv & -4E(1 - E^2)Mr^6 + 12EM^2r^5 - 2E[a^2(1 - E^2) + 3(L_z^2 + Q)]Mr^4 \\
& + 8[a^2E(2 - E^2) + E(L_z^2 + Q) - 2aL_z]M^2r^3 \\
& - 2a[aE[6M^2 + L_z^2 + Q + a^2(1 - E^2)] - 6M^2L_z]Mr^2 \\
& + 4a^2E[Q + (L_z - aE)^2]M^2r - 4a(L_z - aE)[Q + (L_z - aE)^2]M^3, \tag{3.6a}
\end{aligned}$$

$$\begin{aligned}
c_{12}(Q, E, L_z, r) \equiv & -4L_z(1 - E^2)Mr^4 + 16(1 - E^2)(L_z - aE)M^2r^3 \\
& + 2[L_z[a^2(1 - E^2) + L_z^2 + Q] - 6M^2(L_z - aE)]Mr^2 \\
& - 4L_z[Q + (L_z - aE)^2]M^2r + 4(L_z - aE)[Q + (L_z - aE)^2]M^3, \tag{3.6b}
\end{aligned}$$

$$c_{21}(Q, E, L_z, r) \equiv 2Er^5 - 6EMr^4 + 4a^2Er^3 + 2a(L_z - 2aE)Mr^2 + 2a^4Er - 2a^3(L_z - aE)M, \tag{3.6c}$$

$$c_{22}(Q, E, L_z, r) \equiv 2aEMr^2 - 2a^2L_zr + 2a^2(L_z - aE)M, \tag{3.6d}$$

$$\begin{aligned}
d(Q, E, L_z, r) \equiv & -2(1 - E^2)Mr^4 + 8(1 - E^2)M^2r^3 + [Q + L_z^2 - 5a^2(1 - E^2) - 6M^2]Mr^2 \\
& + 2[a^2(3 - E^2) + 2aEL_z - (L_z^2 + Q)]M^2r \\
& + 2(L_z^2 + Q)M^3 - 4aEL_zM^3 + a^2(2E^2M^2 - L_z^2 - Q)M - a^4(1 - E^2)M. \tag{3.6e}
\end{aligned}$$

By determining  $\dot{E}$  and  $\dot{L}_z$ , we determine  $\dot{Q}$  and  $\dot{r}$ , fully fixing the evolution of the particle's orbit. In particular, the rate of change of the inclination angle is

$$i = -\frac{d(\cos \iota)/dt}{1 - \cos^2 \iota}, \tag{3.7}$$

where

$$\frac{d(\cos \iota)}{dt} = \frac{1}{\sqrt{L_z^2 + Q}} \left[ \dot{L}_z - \left( \frac{L_z}{2} \right) \frac{2L_z\dot{L}_z + \dot{Q}}{L_z^2 + Q} \right]. \tag{3.8}$$

## B. Adiabaticity

In this section, we impose adiabaticity on the orbiting particle and show that it constrains the mass ratio of the system. We first impose adiabaticity on motion in the weak field of the black hole ( $r \gg M$ ), and then impose adiabaticity on motion in the strong field ( $r \sim M$ ).

### 1. Weak-field radiation reaction

In the weak-field, a post-Newtonian expansion suffices to calculate the radiated energy and angular momentum. Ryan [38] shows that such a post-Newtonian expansion leads to the following results for the change in the orbital radius and inclination angle:

$$\begin{aligned}
\dot{r}_{\text{weak}} &= -\frac{64}{5} \frac{\mu}{M} \left( \frac{M}{r} \right)^3, \\
\dot{\iota}_{\text{weak}} &= \frac{244}{15} \frac{\mu}{M^2} \frac{a}{M} \left( \frac{M}{r} \right)^{11/2} \sin \iota \simeq \frac{244}{15} \frac{\mu}{M^2} \frac{a}{M} \left( \frac{M}{r} \right)^{11/2} \iota. \tag{3.9}
\end{aligned}$$

In the weak-field,  $T_\theta \simeq 2\pi\sqrt{r^3/M} + O(a)$  [44]. Putting all of this together, we find to leading order

$$\begin{aligned}
\frac{\dot{r}_{\text{weak}}T_\theta}{r} &\simeq \frac{128\pi}{5} \frac{\mu}{M} \left( \frac{M}{r} \right)^{5/2}, \\
\frac{\dot{\iota}_{\text{weak}}T_\theta}{\iota} &\simeq \frac{488\pi}{15} \frac{\mu}{M} \frac{a}{M} \left( \frac{M}{r} \right)^4. \tag{3.10}
\end{aligned}$$

Now impose adiabaticity: the condition  $\dot{r}_{\text{weak}}T_\theta/r \ll 1$  leads to the condition

$$\frac{\mu}{M} \ll \frac{5}{128\pi} \left(\frac{r}{M}\right)^{5/2}, \quad (3.11)$$

and  $i_{\text{weak}} T_\theta / \iota \ll 1$  leads to

$$\frac{\mu}{M} \ll \frac{15}{488\pi} \left(\frac{r}{M}\right)^4. \quad (3.12)$$

Since, by definition,  $\mu/M \leq 1/4$ , Eqs. (3.11) and (3.12) are *always* satisfied in the weak-field. Weak-field radiation reaction is always adiabatic, regardless of the mass ratio. This is not surprising.

## 2. Strong-field radiation reaction

In the strong-field, we do not know *a priori*  $\dot{E}$  and  $\dot{L}_z$ . Nonetheless, we would like to understand what constraints adiabaticity places on the mass ratio, so we must at least estimate  $\dot{E}$  and  $\dot{L}_z$ . Ryan [38] gives the following quadrupole-order formulae, valid in the weak field:

$$\begin{aligned} \dot{E}^{\text{quad}} &= -\frac{32}{5} \left(\frac{\mu}{M}\right)^2 \left(\frac{M}{r}\right)^5 \left[ 1 - \frac{73}{12} \frac{a}{M} \left(\frac{M}{r}\right)^{3/2} \cos \iota \right], \\ \dot{L}_z^{\text{quad}} &= -\frac{32M}{5} \left(\frac{\mu}{M}\right)^2 \left(\frac{M}{r}\right)^{7/2} \left[ \cos \iota + \frac{61}{24} \frac{a}{M} \left(\frac{M}{r}\right)^{3/2} (1 - 3 \cos^2 \iota) \right]. \end{aligned} \quad (3.13)$$

(These are the rates of change of the *physical* energy and angular momentum, not the specific energy and angular momentum used in the rest of this paper.) We will take the *ansatz* that these formulae are valid up to factors of order unity even in the strong field. (Detailed analysis shows that this *ansatz* is reasonable; cf. Tables I – IV.)

Consider prograde, equatorial orbits with  $a = M$ ,  $r = (1 + \epsilon)M$ : a particle orbiting just barely outside the event horizon of an extreme Kerr black hole. In this limit,

$$T_\theta = M \left[ \frac{4\pi}{\epsilon} \sqrt{\frac{2}{3}} + \frac{22\pi}{3} \sqrt{\frac{2}{3}} + O(\epsilon) \right]. \quad (3.14)$$

Solving Eq. (3.5) using the quadrupole formulae (3.13) with  $a = M$ ,  $r = (1 + \epsilon)M$  and expanding in  $\epsilon$  gives

$$\dot{r} \simeq -\frac{584}{5\sqrt{3}\epsilon} + \frac{13657}{15\sqrt{3}} + O(\epsilon). \quad (3.15)$$

Combining these results and imposing the adiabatic condition  $\dot{r} T_\theta / r \ll 1$ , we obtain

$$\frac{\mu}{M} \ll \frac{15\epsilon^2}{2336\sqrt{2}\pi} + O(\epsilon^3). \quad (3.16)$$

This is a very stringent requirement. Since our calculation will assume that adiabaticity holds over the entire evolution, Eq. (3.16) tells us that our results in the strong field will only be astrophysically meaningful when applied to systems for which the mass ratio is very extreme. (Cutler, Kennefick, and Poisson showed a similar condition holds as an orbiting point particle approaches the innermost stable circular orbit of the Schwarzschild spacetime [31].)

## IV. RADIATION REACTION: THE TEUKOLSKY AND SASAKI-NAKAMURA EQUATIONS

### A. The Teukolsky equation

We use a formalism based on the Teukolsky equation to study radiation reaction. The Teukolsky equation describes the behavior of the Weyl curvature component  $\psi_4$ , which encapsulates all information about the gravitational radiation flux at infinity and at the event horizon. Teukolsky showed [3] that the multipolar decomposition

$$\psi_4 = \frac{1}{(r - ia \cos \theta)^4} \int_{-\infty}^{\infty} d\omega \sum_{lm} R_{lm\omega}(r) {}_{-2}S_{lm}^{a\omega}(\theta) e^{im\phi} e^{-i\omega t} \quad (4.1)$$

separates the evolution equation for  $\psi_4$ . The function  ${}_{-2}S_{lm}^{a\omega}(\theta)$  is a spin-weighted spheroidal harmonic; it is discussed in Appendix A. The radial function  $R_{lm\omega}(r)$  obeys the Teukolsky equation:

$$\Delta^2 \frac{d}{dr} \left( \frac{1}{\Delta} \frac{dR_{lm\omega}}{dr} \right) - V(r)R_{lm\omega}(r) = -\mathcal{T}_{lm\omega}(r). \quad (4.2)$$

The potential is

$$V(r) = -\frac{K^2 + 4i(r-M)K}{\Delta} + 8i\omega r + \lambda, \quad (4.3)$$

where  $K = (r^2 + a^2)\omega - ma$ , and<sup>3</sup>  $\lambda \equiv \mathcal{E}_{lm} - 2am\omega + a^2\omega^2 - 2$ . The number  $\mathcal{E}_{lm}$  is the eigenvalue of the spheroidal harmonic; see Appendix A for details.

The homogeneous Teukolsky equation admits two independent solutions,  $R_{lm\omega}^H$  and  $R_{lm\omega}^\infty$ , with the following asymptotic values:

$$\begin{aligned} R_{lm\omega}^H &= B_{lm\omega}^{\text{hole}} \Delta^2 e^{-ip_{m\omega}r^*}, & r \rightarrow r_+ \\ R_{lm\omega}^H &= B_{lm\omega}^{\text{out}} r^3 e^{i\omega r^*} + \frac{B_{lm\omega}^{\text{in}}}{r} e^{-i\omega r^*}, & r \rightarrow \infty; \end{aligned} \quad (4.4)$$

and

$$\begin{aligned} R_{lm\omega}^\infty &= D_{lm\omega}^{\text{out}} e^{ip_{m\omega}r^*} + D_{lm\omega}^{\text{in}} \Delta^2 e^{-ip_{m\omega}r^*}, & r \rightarrow r_+ \\ R_{lm\omega}^\infty &= D_{lm\omega}^\infty r^3 e^{i\omega r^*}, & r \rightarrow \infty. \end{aligned} \quad (4.5)$$

We have introduced  $p_{m\omega} = \omega - m\omega_+$ , where  $\omega_+ \equiv a/2Mr_+$  is the ‘‘angular velocity of the horizon’’ (the angular velocity with which inertial observers at the horizon are seen to rotate due to frame dragging [43]), and the ‘‘tortoise coordinate’’

$$r^*(r) = r + \frac{2Mr_+}{r_+ - r_-} \ln \frac{r - r_+}{2M} - \frac{2Mr_-}{r_+ - r_-} \ln \frac{r - r_-}{2M}, \quad (4.6)$$

which is derived from the rule  $dr^*/dr = (r^2 + a^2)/\Delta$ . (In these relations,  $r_\pm = M \pm \sqrt{M^2 - a^2}$ ; recall that  $r_+$  is the coordinate of the event horizon.) With these solutions and using the theory of Green’s functions [48], the general solution of the Teukolsky equation can be written

$$R_{lm\omega}(r) = Z_{lm\omega}^H(r)R_{lm\omega}^\infty(r) + Z_{lm\omega}^\infty(r)R_{lm\omega}^H(r), \quad (4.7)$$

where

$$\begin{aligned} Z_{lm\omega}^H(r) &= \frac{1}{2i\omega B_{lm\omega}^{\text{in}} D_{lm\omega}^\infty} \int_{r_+}^r dr' \frac{R_{lm\omega}^H(r') \mathcal{T}_{lm\omega}(r')}{\Delta(r')^2}, \\ Z_{lm\omega}^\infty(r) &= \frac{1}{2i\omega B_{lm\omega}^{\text{in}} D_{lm\omega}^\infty} \int_r^\infty dr' \frac{R_{lm\omega}^\infty(r') \mathcal{T}_{lm\omega}(r')}{\Delta(r')^2}. \end{aligned} \quad (4.8)$$

By construction,  $Z_{lm\omega}^H(r \rightarrow r_+) = Z_{lm\omega}^\infty(r \rightarrow \infty) = 0$ . Defining  $Z_{lm\omega}^H \equiv Z_{lm\omega}^H(r \rightarrow \infty)$ ,  $Z_{lm\omega}^\infty \equiv Z_{lm\omega}^\infty(r \rightarrow r_+)$ , the asymptotic radial solutions are

$$\begin{aligned} R_{lm\omega}(r \rightarrow \infty) &= Z_{lm\omega}^H D_{lm\omega}^\infty r^3 e^{i\omega r^*}, \\ R_{lm\omega}(r \rightarrow r_+) &= Z_{lm\omega}^\infty B_{lm\omega}^{\text{hole}} \Delta^2 e^{-ip_{m\omega}r^*}. \end{aligned} \quad (4.9)$$

This solution is purely ingoing at the horizon and purely outgoing at infinity, which is physically correct. It is convenient to absorb the factors  $D_{lm\omega}^\infty$  and  $B_{lm\omega}^{\text{hole}}$  into  $Z_{lm\omega}^H$  and  $Z_{lm\omega}^\infty$  respectively, and rewrite Eq. (4.8):

---

<sup>3</sup>For general spin fields,  $\lambda = \mathcal{E}_{lm} - 2am\omega + a^2\omega^2 - s(s+1)$ ; however, we have specialized to  $s = -2$ .

$$\begin{aligned}
Z_{lm\omega}^H(r) &= \frac{1}{2i\omega B_{lm\omega}^{\text{in}}} \int_{r_+}^r dr' \frac{R_{lm\omega}^H(r') \mathcal{T}_{lm\omega}(r')}{\Delta(r')^2}, \\
Z_{lm\omega}^\infty(r) &= \frac{B_{lm\omega}^{\text{hole}}}{2i\omega B_{lm\omega}^{\text{in}} D_{lm\omega}^\infty} \int_r^\infty dr' \frac{R_{lm\omega}^\infty(r') \mathcal{T}_{lm\omega}(r')}{\Delta(r')^2}.
\end{aligned} \tag{4.10}$$

From these asymptotic solutions, we construct the energy and angular momentum flux due to gravitational radiation that goes to infinity and down the event horizon. First, note that the particle's motion is describable as a set of harmonics of the frequencies  $\Omega_\theta$  and  $\Omega_\phi$ , and define

$$\omega_{mk} = m\Omega_\phi + k\Omega_\theta. \tag{4.11}$$

Then, decompose the  $\omega$  dependence of  $Z_{lm\omega}^H$  and  $Z_{lm\omega}^\infty$  as

$$\begin{aligned}
Z_{lm\omega}^H &= \sum_k Z_{lmk}^H \delta(\omega - \omega_{mk}), \\
Z_{lm\omega}^\infty &= \sum_k Z_{lmk}^\infty \delta(\omega - \omega_{mk}).
\end{aligned} \tag{4.12}$$

The coefficients  $Z_{lmk}^{H,\infty}$  fully determine the energy and angular momentum fluxes.

### 1. Fluxes as $r \rightarrow \infty$

As  $r \rightarrow \infty$ ,

$$\psi_4(r \rightarrow \infty) \rightarrow \frac{1}{2} (\ddot{h}_+ - i\ddot{h}_\times). \tag{4.13}$$

The energy flux in gravitational waves, from the Isaacson stress-energy tensor [20], is

$$\left( \frac{dE}{dAdt} \right)_{r \rightarrow \infty}^{\text{rad}} = \frac{1}{16\pi} \left\langle \left( \frac{\partial h_+}{\partial t} \right)^2 + \left( \frac{\partial h_\times}{\partial t} \right)^2 \right\rangle, \tag{4.14}$$

where the angle brackets denote averaging over several wavelengths. Combining Eqs. (4.1), (4.9), (4.12), and (4.14), we obtain

$$\begin{aligned}
\left( \frac{dE}{dt} \right)_{r \rightarrow \infty}^{\text{rad}} &= \sum_{lmk} \frac{|Z_{lmk}^H|^2}{4\pi\omega_{mk}^2}, \\
\left( \frac{dL_z}{dt} \right)_{r \rightarrow \infty}^{\text{rad}} &= \sum_{lmk} \frac{m|Z_{lmk}^H|^2}{4\pi\omega_{mk}^3}.
\end{aligned} \tag{4.15}$$

### 2. Fluxes as $r \rightarrow r_+$

The energy and angular momentum flux at the horizon can be calculated by measuring the rate at which the event horizon's area increases as radiation falls into it, following the prescription of [21] as described in [46]. The result is

$$\begin{aligned}
\left( \frac{dE}{dt} \right)_{r \rightarrow r_+}^{\text{rad}} &= \sum_{lmk} \alpha_{lmk} \frac{|Z_{lmk}^\infty|^2}{4\pi\omega_{mk}^2}, \\
\left( \frac{dL_z}{dt} \right)_{r \rightarrow r_+}^{\text{rad}} &= \sum_{lmk} \alpha_{lmk} \frac{m|Z_{lmk}^\infty|^2}{4\pi\omega_{mk}^3}.
\end{aligned} \tag{4.16}$$

The coefficient  $\alpha_{lmk}$  is found by transforming from Kinnerley's null tetrad (used to construct  $\psi_4$ ) to the Hawking-Hartle null tetrad [21] (which is well-behaved at the Kerr event horizon); see [46] for details. It is given by

$$\alpha_{lmk} = \frac{256(2Mr_+)^5 p_{mk}(p_{mk}^2 + 4\varepsilon^2)(p_{mk}^2 + 16\varepsilon^2)\omega_{mk}^3}{|C_{lmk}|^2}, \quad (4.17)$$

with  $\varepsilon = \sqrt{M^2 - a^2}/4Mr_+$ , and

$$|C_{lmk}|^2 = [(\lambda + 2)^2 + 4a\omega_{mk} - 4a^2\omega_{mk}^2] (\lambda^2 + 36ma\omega_{mk} - 36a^2\omega_{mk}^2) + (2\lambda + 3)(96a^2\omega_{mk}^2 - 48ma\omega_{mk}) + 144\omega_{mk}^2(M^2 - a^2). \quad (4.18)$$

In order to calculate all of the fluxes and from them deduce the evolution of the particle's orbit, we need a method to calculate the coefficients  $Z_{lmk}^H$  and  $Z_{lmk}^\infty$ . This, in turn, requires us to calculate the coefficients  $B_{lmk}^{\text{in}}$ ,  $B_{lmk}^{\text{hole}}$ , and  $D_{lmk}^\infty$ . To do so, we use the Sasaki-Nakamura equation.

## B. The Sasaki-Nakamura equation

In principle, one should be able to calculate all the necessary coefficients directly from the Teukolsky equation. Consider in particular  $B_{lmk}^{\text{in}}$ . From Eq. (4.4), we know that we should be able to start with a purely ingoing pulse of radiation at the event horizon with unit amplitude; we should then be able to use the Teukolsky equation to integrate out very far, and read off the ratio  $B_{lmk}^{\text{in}}/B_{lmk}^{\text{hole}}$  (as well as  $B_{lmk}^{\text{out}}/B_{lmk}^{\text{hole}}$ ). This approach does not work well in a practical numerical implementation. The reason is that by Eq. (4.4) the outgoing solution grows with a coefficient  $r^4$  relative to the ingoing coefficient — it completely swamps the ingoing solution, making it impossible to read off  $B_{lmk}^{\text{in}}$  with any kind of accuracy.

The fundamental reason for this difficulty is that the Teukolsky equation's potential  $V(r)$  is long ranged. A solution to this difficulty was given by Sasaki and Nakamura [42], who discovered a transformation that takes the Teukolsky function  $R(r)$ , governed by an equation with long-ranged potential, to the Sasaki-Nakamura function  $X(r)$ , governed by an equation with short-ranged potential.

The Sasaki-Nakamura equation is

$$\frac{d^2 X_{lmk}}{dr^{*2}} - F(r) \frac{dX_{lmk}}{dr^*} - U(r) X_{lmk} = 0. \quad (4.19)$$

The functions  $F(r)$  and  $U(r)$  are shown explicitly in Appendix B. Like the Teukolsky equation, the Sasaki-Nakamura equation admits two solutions, whose asymptotic forms are

$$\begin{aligned} X_{lmk}^H &= e^{-ip_{mk}r^*}, & r \rightarrow r_+, \\ X_{lmk}^H &= A_{lmk}^{\text{out}} \bar{P}(r) e^{i\omega_{mk}r^*} + A_{lmk}^{\text{in}} P(r) e^{-i\omega_{mk}r^*}, & r \rightarrow \infty; \end{aligned} \quad (4.20)$$

and

$$\begin{aligned} X_{lmk}^\infty &= C_{lmk}^{\text{out}} e^{ip_{mk}r^*} + C_{lmk}^{\text{in}} e^{-ip_{mk}r^*}, & r \rightarrow r_+, \\ X_{lmk}^\infty &= \bar{P}(r) e^{i\omega_{mk}r^*}, & r \rightarrow \infty. \end{aligned} \quad (4.21)$$

The function

$$P(r) = 1 + \frac{\mathcal{A}}{\omega r} + \frac{\mathcal{B}}{(\omega r)^2} + \frac{\mathcal{C}}{(\omega r)^3} \quad (4.22)$$

allows us to more accurately describe the behavior of  $X^{H,\infty}$  near infinity. Inserting  $X^{H,\infty}$  into the Sasaki-Nakamura equation (4.19), and taking the limit  $r \rightarrow \infty$ , we read off  $\mathcal{A}$ ,  $\mathcal{B}$ , and  $\mathcal{C}$ :

$$\mathcal{A} = -\frac{i}{2}(\lambda + 2 + 2am\omega), \quad (4.23a)$$

$$\mathcal{B} = -\frac{1}{8} [(\lambda + 2)^2 - (\lambda + 2)(2 - 4am\omega) - 4[am\omega + 3iM\omega - am\omega(am\omega + 2IM\omega)]] , \quad (4.23b)$$

$$\mathcal{C} = -\frac{i}{6} [4am\omega + \mathcal{B}(\lambda - 4 + 2am\omega + 8iM\omega) + 12(M\omega)^2 - 2\mathcal{A}\lambda M\omega - (a\omega)^2(\lambda - 3 + m^2 + 2am\omega)] . \quad (4.23c)$$

In the limit  $a \rightarrow 0$ , Eqs. (4.23a)–(4.23c) reduce to the results given in [28].

One transforms from the Sasaki-Nakamura function to the Teukolsky function with the rule



$$R_{lmk}^{H,\infty} = \frac{1}{\eta} \left[ \left( \alpha + \frac{\beta_{,r}}{\Delta} \right) \chi_{lmk}^{H,\infty} - \frac{\beta}{\Delta} \chi_{lmk,r}^{H,\infty} \right], \quad (4.24)$$

where  $\chi_{lmk}^{H,\infty} = X_{lmk}^{H,\infty} \Delta / \sqrt{r^2 + a^2}$ . From this rule follow relations for the various coefficients:

$$B_{lmk}^{\text{in}} = -\frac{A_{lmk}^{\text{in}}}{4\omega_{mk}^2}, \quad (4.25a)$$

$$D_{lmk}^{\infty} = -\frac{4\omega_{mk}^2}{c_0}, \quad (4.25b)$$

$$B_{lmk}^{\text{hole}} = \frac{1}{d_{lm\omega}}, \quad \text{where} \quad (4.25c)$$

$$d_{lm\omega} = \sqrt{2Mr_+} [(8 - 24iM\omega - 16M^2\omega^2)r_+^2 + (12iam - 16M + 16amM\omega + 24iM^2\omega)r_+ - 4a^2m^2 - 12iamM + 8M^2]. \quad (4.25d)$$

The functions  $\alpha$ ,  $\beta$ , and  $\eta$  and the coefficient  $c_0$  are given in Appendix B. The quantity  $B_{lmk}^{\text{hole}}$  is taken from Ref. [32].

The only coefficient which must be calculated numerically is  $A_{lmk}^{\text{in}}$ . This is quite reasonable: from Eq. (4.20), we begin with a unit amplitude, purely ingoing pulse of radiation near the event horizon and integrate outward to read off  $A^{\text{in}}$ . As  $r \rightarrow \infty$ , the outgoing piece of  $X_{lmk}^H$  remains of constant amplitude, so  $A_{lmk}^{\text{in}}$  is easy to extract. This prescription is sufficient to calculate the solutions to the homogeneous Teukolsky equation.

### C. The source term

The next part of the analysis is to compute the source of the Teukolsky equation. This term is given by [49]

$$\mathcal{T}_{lm\omega}(r) = 4 \int d\Omega dt \frac{\Sigma}{\rho^4} (B_2' + B_2^{*'})_{-2} S_{lm}^{a\omega}(\theta) e^{-im\phi} e^{i\omega t}, \quad (4.26)$$

where the functions  $B_2'$  and  $B_2^{*'}$  are

$$B_2' = -\frac{\rho^8 \bar{\rho}}{2} L_{-1} [\rho^{-4} L_0 (\rho^{-2} \bar{\rho}^{-1} T_{nn})] + \frac{\Delta^2 \rho^8 \bar{\rho}}{2\sqrt{2}} L_{-1} [\rho^{-4} \bar{\rho}^2 J_+ (\rho^{-2} \bar{\rho}^{-2} \Delta^{-1} T_{n\bar{m}})], \quad (4.27)$$

$$B_2^{*'} = \frac{\Delta^2 \rho^8 \bar{\rho}}{2\sqrt{2}} J_+ [\rho^{-4} \bar{\rho}^2 \Delta^{-1} L_{-1} (\rho^{-2} \bar{\rho}^{-2} T_{n\bar{m}})] - \frac{\Delta^2 \rho^8 \bar{\rho}}{4} J_+ [\rho^{-4} J_+ (\rho^{-2} \bar{\rho} T_{\bar{m}\bar{m}})]. \quad (4.28)$$

Here,  $\rho = -1/(r - ia \cos \theta)$ ,  $\bar{\rho} = -1/(r + ia \cos \theta)$  (note that  $\rho$  and  $\bar{\rho}$  have the opposite sign from that used in, for example, [32]; this is the sign convention used in, for example, [3]). The differential operators  $J_+$  and  $L_s$  are

$$J_+ = \partial_r + \frac{iK(r)}{\Delta}, \quad (4.29)$$

$$L_s = \partial_\theta + m \csc \theta - a\omega \sin \theta + s \cot \theta.$$

The quantities  $T_{nn}$ ,  $T_{n\bar{m}}$  and  $T_{\bar{m}\bar{m}}$  are projections of the stress-energy tensor for the orbiting point particle onto the Newman-Penrose null-tetrad legs  $\mathbf{n}$ ,  $\bar{\mathbf{m}}$ :  $T_{nn} = T^{\alpha\beta} n_\alpha n_\beta$ , etc. For a point particle moving in the Kerr spacetime,

$$T^{\alpha\beta}(x) = \mu \int d\tau u^\alpha u^\beta \delta^{(4)} [x - z(\tau)]$$

$$= \mu \int d\tau u^\alpha u^\beta (-g)^{1/2} \delta [t - t(\tau)] \delta [r - r(\tau)] \delta [\theta - \theta(\tau)] \delta [\phi - \phi(\tau)]. \quad (4.30)$$

Here,  $x$  is an arbitrary spacetime point,  $\tau$  is proper time measured by the moving particle,  $z(\tau)$  is the particle's worldline, and  $(-g)^{1/2} = \Sigma \sin \theta$  is the factor which converts coordinate volume to proper volume ( $g$  is the determinant of the covariant components of the Kerr metric.)

As discussed in the Introduction and in Sec. III B, the true world line of the particle is given by a Kerr geodesic plus radiation reaction corrections. Since we do not yet know these corrections, we use the zeroth order geodesic motion to write down this stress-energy tensor. Performing the integral, we find

$$T^{\alpha\beta}(r, \theta, \phi, t) = \mu \frac{u^\alpha u^\beta}{\Sigma \sin \theta \dot{t}} \delta(r - r_0) \delta[\theta - \theta(t)] \delta[\phi - \phi(t)] . \quad (4.31)$$

This is specialized to circular orbits of radius  $r_0$ .

Next, project this stress-energy tensor onto the Newman-Penrose null tetrad. From [22],

$$\begin{aligned} n_\alpha &= \frac{1}{2} \left( \frac{\Delta}{\Sigma}, 1, 0, -\frac{a\Delta \sin^2 \theta}{\Sigma} \right) , \\ \bar{m}_\alpha &= \frac{\rho}{\sqrt{2}} (ia \sin \theta, 0, \Sigma, -i(r^2 + a^2) \sin \theta) . \end{aligned} \quad (4.32)$$

It is useful to write the projected stress-energy tensor components in the form

$$T_{ab} = \frac{C_{ab}}{\sin \theta} \delta(r - r_0) \delta[\theta - \theta(t)] \delta[\phi - \phi(t)] . \quad (4.33)$$

Setting  $\dot{r} = 0$ , performing the projection, and using Eqs. (2.1b)–(2.1d) yields

$$\begin{aligned} C_{nn} &= \frac{\mu}{4\Sigma^3 \dot{t}} [E(r^2 + a^2) - aL_z]^2 , \\ C_{n\bar{m}} &= \frac{\mu\rho}{2\sqrt{2}\Sigma^2 \dot{t}} [E(r^2 + a^2) - aL_z] \left[ i \sin \theta \left( aE - \frac{L_z}{\sin^2 \theta} \right) + \Theta \right] , \\ C_{\bar{m}\bar{m}} &= \frac{\mu\rho^2}{2\Sigma \dot{t}} \left[ i \sin \theta \left( aE - \frac{L_z}{\sin^2 \theta} \right) + \Theta \right]^2 . \end{aligned} \quad (4.34)$$

The function  $\Theta$  is given in Eq. (2.1b). As written, its sign is ambiguous, depending on whether the particle is ascending ( $\theta$  decreasing) or descending ( $\theta$  increasing). We take  $\Theta$  to be positive, and define

$$\begin{aligned} C_{nn}^\pm &= \frac{\mu}{4\Sigma^3 \dot{t}} [E(r^2 + a^2) - aL_z]^2 = C_{nn} , \\ C_{n\bar{m}}^\pm &= \frac{\mu\rho}{2\sqrt{2}\Sigma^2 \dot{t}} [E(r^2 + a^2) - aL_z] \left[ i \sin \theta \left( aE - \frac{L_z}{\sin^2 \theta} \right) \pm \Theta \right] , \\ C_{\bar{m}\bar{m}}^\pm &= \frac{\mu\rho^2}{2\Sigma \dot{t}} \left[ i \sin \theta \left( aE - \frac{L_z}{\sin^2 \theta} \right) \pm \Theta \right]^2 . \end{aligned} \quad (4.35)$$

These quantities will be used later in order to break this ambiguity when computing the source function.

Next use Eqs. (4.27), (4.28), (4.33), and (4.34) to expand Eq. (4.26), and then repeatedly integrate by parts so that no  $\theta$  derivatives are taken of any delta functions. The following identity [22,35] simplifies this integration:

$$\int_0^\pi h(\theta) L_s [g(\theta)] \sin \theta d\theta = - \int_0^\pi g(\theta) L_{1-s}^\dagger [h(\theta)] \sin \theta d\theta , \quad (4.36)$$

where

$$L_s^\dagger = \partial_\theta - m \csc \theta + a\omega \sin \theta + s \cot \theta . \quad (4.37)$$

With moderate effort, we find

$$\begin{aligned} \mathcal{T}_{lm\omega}(r) &= -4 \int dt e^{i[\omega t - m\phi(t)]} \left\{ \frac{\rho^{-2} \bar{\rho}^{-1}}{2} C_{nn} \delta(r - r_0) L_1^\dagger \left[ \rho^{-4} L_2^\dagger (\rho^3 S) \right] \right. \\ &\quad + \frac{\Delta^2 \rho^{-1} \bar{\rho}^2}{\sqrt{2}} J_+ \left[ \rho^{-2} \bar{\rho}^{-2} \Delta^{-1} C_{n\bar{m}} \delta(r - r_0) \right] \left[ ia \sin \theta (\rho - \bar{\rho}) S + L_2^\dagger S \right] \\ &\quad + \frac{\Delta \rho^{-2} \bar{\rho}^{-2}}{2\sqrt{2}} C_{n\bar{m}} \delta(r - r_0) L_2^\dagger \left[ \rho^3 S \partial_r (\rho^{-4} \bar{\rho}^2) \right] \\ &\quad \left. + \frac{\Delta^2 \rho^3}{4} S J_+ \left[ \rho^{-4} J_+ (\rho^{-2} \bar{\rho} C_{\bar{m}\bar{m}} \delta(r - r_0)) \right] \right\} . \end{aligned} \quad (4.38)$$

All functions of  $\theta$  are evaluated at  $\theta(t)$ , the particle's  $\theta$  coordinate at  $t$ . We have written  $S$  as shorthand for  ${}_{-2}S_{lm}^{a\omega}[\theta(t)]$ .

Following [32], it is very convenient to write this in the form

$$\mathcal{T}_{lm\omega}(r) = \int dt \Delta^2 \{ [A_{nn0} + A_{n\bar{m}0} + A_{\bar{m}\bar{m}0}] \delta(r - r_0) + \partial_r ([A_{n\bar{m}1} + A_{\bar{m}\bar{m}1}] \delta(r - r_0)) + \partial_r^2 [A_{\bar{m}\bar{m}2} \delta(r - r_0)] \} . \quad (4.39)$$

From Eq. (4.38), it is not too difficult to work out  $A_{abi}$ :

$$A_{nn0} = -\frac{2\rho^{-3}\bar{\rho}^{-1}C_{nn}}{\Delta^2} \left[ L_1^\dagger L_2^\dagger S + 2ia\rho \sin\theta L_2^\dagger S \right] , \quad (4.40a)$$

$$A_{n\bar{m}0} = -\frac{2\sqrt{2}\rho^{-3}C_{n\bar{m}}}{\Delta} \left[ \left( \frac{iK}{\Delta} - \rho - \bar{\rho} \right) L_2^\dagger S + \left( \frac{iK}{\Delta} + \rho + \bar{\rho} \right) ia \sin\theta S(\rho - \bar{\rho}) \right] , \quad (4.40b)$$

$$A_{\bar{m}\bar{m}0} = S\rho^{-3}\bar{\rho} \left[ \left( \frac{K}{\Delta} \right)^2 + 2i\rho \frac{K}{\Delta} + i\partial_r \left( \frac{K}{\Delta} \right) \right] , \quad (4.40c)$$

$$A_{n\bar{m}1} = -\frac{2\sqrt{2}\rho^{-3}C_{n\bar{m}}}{\Delta} \left[ L_2^\dagger S + ia\rho \sin\theta(\rho - \bar{\rho})S \right] , \quad (4.40d)$$

$$A_{\bar{m}\bar{m}1} = 2S\rho^{-3}\bar{\rho} C_{\bar{m}\bar{m}} \left( \rho - \frac{iK}{\Delta} \right) , \quad (4.40e)$$

$$A_{\bar{m}\bar{m}2} = -S\rho^{-3}\bar{\rho} C_{\bar{m}\bar{m}} . \quad (4.40f)$$

We will refer to quantities  $A_{nn0}^\pm$ ,  $A_{n\bar{m}0}^\pm$ ,  $A_{\bar{m}\bar{m}0}^\pm$ , *etc.*, which are the various  $A_{abi}$  written using Eq. (4.35) rather than Eq. (4.34). Equations (4.34), (4.38), and (4.40a)–(4.40f) completely specify the source for circular orbits.

#### D. Evaluation of the coefficients $Z_{lmk}^H$ and $Z_{lmk}^\infty$

The next step is to substitute this source into Eq. (4.10) and integrate for the coefficients  $Z_{lm\omega}^H$ ,  $Z_{lm\omega}^\infty$ . Thanks to the delta functions, these integrals are trivial; the result is

$$\begin{aligned} Z_{lm\omega}^H &= \frac{1}{2i\omega B_{lmk}^{\text{in}}} \int_{-\infty}^{\infty} dt e^{i[\omega t - m\phi(t)]} \left\{ R_{lm\omega}^H(r_0) [A_{nn0} + A_{n\bar{m}0} + A_{\bar{m}\bar{m}0}] \right. \\ &\quad \left. - \frac{dR_{lm\omega}^H}{dr} \Big|_{r_0} [A_{n\bar{m}1} + A_{\bar{m}\bar{m}1}] + \frac{d^2 R_{lm\omega}^H}{dr^2} \Big|_{r_0} A_{\bar{m}\bar{m}2} \right\} , \\ Z_{lm\omega}^\infty &= -\frac{c_0}{8i\omega^3 d_{lmk} B_{lmk}^{\text{in}}} \int_{-\infty}^{\infty} dt e^{i[\omega t - m\phi(t)]} \left\{ R_{lm\omega}^\infty(r_0) [A_{nn0} + A_{n\bar{m}0} + A_{\bar{m}\bar{m}0}] \right. \\ &\quad \left. - \frac{dR_{lm\omega}^\infty}{dr} \Big|_{r_0} [A_{n\bar{m}1} + A_{\bar{m}\bar{m}1}] + \frac{d^2 R_{lm\omega}^\infty}{dr^2} \Big|_{r_0} A_{\bar{m}\bar{m}2} \right\} . \end{aligned} \quad (4.41)$$

For a numerical implementation, it is not useful to leave this in the form of an integral over infinite domain. For simplicity, write the above integrals as

$$Z_{lm\omega}^{H,\infty} = C^{H,\infty} \int_{-\infty}^{\infty} dt e^{i[\omega t - m\phi(t)]} I^{H,\infty}[r_0, \theta(t)] . \quad (4.42)$$

To bring out the harmonic structure of the source, we would like to write the integrand in the form  $J_{mk}^{H,\infty}(r_0) \exp[i(\omega - m\Omega_\phi - k\Omega_\theta)t]$ . First, define

$$J_m^{H,\infty}[r_0, \theta(t)] = I^{H,\infty}[r_0, \theta(t)] e^{im[\Omega_\phi t - \phi(t)]} . \quad (4.43)$$

From the discussion in Sec. II C, we know that

$$J_m^{H,\infty}[r_0, \theta(t)] = \sum_{k=0}^{\infty} J_{mk}^{H,\infty}(r_0) e^{-ik\Omega_\theta t(\theta)} , \quad (4.44)$$

where

$$J_{mk}^{H,\infty}(r_0) = \frac{1}{T_\theta} \int_0^{T_\theta} dt J_m^{H,\infty}[r_0, \theta(t)] e^{ik\Omega_\theta t}. \quad (4.45)$$

Substituting for  $I^{H,\infty}[r_0, \theta(t)]$  in Eq. (4.42) gives

$$\begin{aligned} Z_{lm\omega}^{H,\infty} &= C^{H,\infty} \sum_{k=0}^{\infty} \int_{-\infty}^{\infty} dt e^{i[\omega - m\Omega_\phi - k\Omega_\theta]t} J_{mk}^{H,\infty}(r_0), \\ &= 2\pi C^{H,\infty} \sum_{k=0}^{\infty} \delta(\omega - \omega_{mk}) J_{mk}^{H,\infty}(r_0). \end{aligned} \quad (4.46)$$

Then use Eq. (4.12) to find

$$Z_{lmk}^{H,\infty} = 2\pi C^{H,\infty} \sum_{k=0}^{\infty} J_{mk}^{H,\infty}(r_0). \quad (4.47)$$

We must next evaluate the number  $J_{mk}^{H,\infty}(r_0)$ . By Eqs. (4.43) and (4.45),

$$J_{mk}^{H,\infty}(r_0) = \frac{1}{T_\theta} \int_0^{T_\theta} dt e^{i[\omega_{mk}t - m\phi(t)]} I^{H,\infty}[r_0, \theta(t)]. \quad (4.48)$$

Because the dependence of  $I_{mk}^{H,\infty}$  on  $t$  is implicit, it is useful to change the integration variable to  $\chi$ . The integrand then picks up a factor  $(d\chi/dt)^{-1}$ . This is well-behaved over the entire domain of the integral [cf. Eq. (2.10)]. Changing to  $\theta$ , for example, would not work well since the factor  $(d\theta/dt)^{-1}$  is singular at the turning points  $\theta_{\max/\min}$ .

Writing  $dt = d\chi (d\chi/dt)^{-1}$  and combining all of the results of this section, gives

$$Z_{lmk}^H = \frac{\pi}{i\omega_{mk} T_\theta B_{lmk}^{\text{in}}} \sum_{\pm} \int_0^\pi d\chi \frac{\gamma + a^2 E z(\chi)}{\sqrt{\beta[z_+ - z(\chi)]}} e^{\pm i[\omega_{mk}t(\chi) - m\phi(\chi)]} \pm I_{lmk}^H[r_0, z(\chi)], \quad (4.49)$$

$$Z_{lmk}^\infty = -\frac{\pi c_0}{4i\omega_{mk}^3 d_{lm\omega} T_\theta B_{lmk}^{\text{in}}} \sum_{\pm} \int_0^\pi d\chi \frac{\gamma + a^2 E z(\chi)}{\sqrt{\beta[z_+ - z(\chi)]}} e^{\pm i[\omega_{mk}t(\chi) - m\phi(\chi)]} \pm I_{lmk}^\infty[r_0, z(\chi)], \quad (4.50)$$

where

$$\pm I_{lmk}^{H,\infty}[r_0, z(\chi)] = R_{lm\omega}^{H,\infty}(r_0) [A_{nn0}^\pm + A_{n\bar{m}0}^\pm + A_{\bar{m}\bar{m}0}^\pm] - \left. \frac{dR_{lm\omega}^{H,\infty}}{dr} \right|_{r_0} [A_{n\bar{m}1}^\pm + A_{\bar{m}\bar{m}1}^\pm] + \left. \frac{d^2 R_{lm\omega}^{H,\infty}}{dr^2} \right|_{r_0} A_{\bar{m}\bar{m}2}^\pm. \quad (4.51)$$

The coefficients  $Z_{lmk}^{H,\infty}$  obey a useful symmetry between harmonics  $(m, k)$  and  $(-m, -k)$ . From Eqs. (4.49)–(4.51) and by inspection of the Teukolsky equation [Eq. (4.2)], it is apparent that  $Z_{l-m-k}^{H,\infty} = e^{i\alpha} \bar{Z}_{lmk}^{H,\infty}$ , where  $\alpha$  is some phase factor (as yet undetermined). It is simple to determine this phase factor in the Schwarzschild limit. Because of spherical symmetry, waveforms emitted by a particle orbiting at some angle  $\iota$  to the equator of a Schwarzschild hole and observed in the equatorial plane are equivalent to those emitted by a particle orbiting in the equatorial plane and observed at an angle  $-\iota$ . Equating the expressions for the waveforms in these two cases yields  $e^{i\alpha} = (-1)^{k+l}$ , so that

$$Z_{l-m-k}^{H,\infty} = (-1)^{k+l} \bar{Z}_{lmk}^{H,\infty}. \quad (4.52)$$

This factor in fact arises from the rotation properties of the spin-weighted spherical harmonics. Because we generate spheroidal harmonics as a sum of spherical harmonics, Eq. (4.52) holds for Kerr black holes as well. Hence, we need only consider  $k \geq 0$ .

## V. NUMERICAL IMPLEMENTATION AND VALIDATION

In this section, we first describe the structure and methods of the numerical code that was used to study circular orbit radiation reaction. We next present results of certain “sanity checks” that were run to make sure that, in the proper limits, the code reproduces well-known results.

## A. Code implementation

The numerical code can be broken into two pieces: a set of “harmonic” routines which calculate the coefficients  $Z_{lmk}^H$  and  $Z_{lmk}^\infty$  (and thence the energy and angular momentum fluxes), and a “driver” routine which repeatedly calls the harmonic routines and determines when they have “converged” (as defined below) to give the fluxes of energy and angular momentum emitted by that particular orbit.

The driving algorithm has the following structure:

1. Choose the orbital radius  $r$  and angular momentum  $L_z$ . From this, compute the orbital energy  $E$  and Carter constant  $Q$  via Eqs. (2.8) and (2.9), and also the inclination angle  $\iota$  via Eq. (2.5).
2. Loop on the harmonic index  $l$ , starting with  $l = 2$ , until the  $l$ -convergence criterion discussed below is satisfied.
3. For each value of  $l$ , loop on the index  $m \in [-l, \dots, l]$ .
4. For each value of  $m$ , loop on the index  $k$  until the  $k$ -convergence criterion discussed below is satisfied. Because of the symmetry condition Eq. (4.52), consider only  $k \geq 0$ .
5. Compute the frequency  $\omega_{mk} = m\Omega_\phi + k\Omega_\theta$  using Eqs. (2.14) and (2.19).
6. Compute the spheroidal harmonic expansion coefficients  $b_j^{a\omega}$  [cf. Eq. (A2)].
7. Compute the coefficients  $Z_{lmk}^{H,\infty}$ . This is described separately below.
8. Compute the energy and angular momentum fluxes to infinity and down the hole via Eqs. (4.15) and (4.16).
9. Check the convergence of the  $k$  loop. The convergence test implemented here is to check whether  $\dot{E}_{lmk}^{\text{rad}} < \epsilon_k \max_k \dot{E}_{lmk}^{\text{rad}}$  (where  $\dot{E}_{lmk}^{\text{rad}} = \dot{E}_{lmk}^H + \dot{E}_{lmk}^\infty$ , and  $\max_k \dot{E}_{lmk}^{\text{rad}}$  is the largest value of  $\dot{E}_{lmk}^{\text{rad}}$  over all  $k$  values). The value of  $\epsilon_k$  is discussed in greater detail in Sec. VI. When this condition is met for three successive  $k$  values, the  $k$ -loop is ended. Otherwise, increase  $k$  by one and repeat the  $k$ -loop.
10. If  $m = l$ , terminate the  $m$ -loop, else increase  $m$  by one and repeat.
11. Check the convergence of the  $l$  loop. The convergence test implemented here is to check whether  $\dot{E}_l^{\text{rad}} < \epsilon_l \max_l \dot{E}_l^{\text{rad}}$  (where  $\dot{E}_l^{\text{rad}} = \sum_{mk} \dot{E}_{lmk}^{\text{rad}}$ , and  $\max_l \dot{E}_l^{\text{rad}}$  is the largest value of  $\dot{E}_l^{\text{rad}}$  over all  $l$  values). We have typically used  $\epsilon_l = 10 \times \epsilon_k$ . When this condition is met for three successive  $l$  values, the  $l$ -loop is ended. Otherwise, increase  $l$  by one and repeat.
12. Compute the total change in the angular momentum and energy of the particle:

$$\dot{E} = - \sum_l \dot{E}_l^{\text{rad}}, \quad \dot{L}_z = - \sum_l \dot{L}_{z;l}^{\text{rad}}. \quad (5.1)$$

13. Compute the total change in the particle’s radius, Carter constant and inclination angle using Eqs. (3.5)–(3.7).
14. Compute the gravitational waveform:

$$h_+(\theta, \phi, t) - ih_\times(\theta, \phi, t) = \sum_{lmk} \frac{1}{\omega_{mk}^2} Z_{lmk}^H - 2S_{lm}^{a\omega_{mk}}(\theta) e^{i(m\phi - \omega t)}. \quad (5.2)$$

For a given orbit with some radius and inclination angle  $(r, \iota)$ , this algorithm gives the orbit’s gravitational waveform and the direction  $(\hat{r}, \hat{i})$  in which radiation reaction drives it to a new orbit.

The “harmonic” routines which calculate the coefficients  $Z_{lmk}^{H,\infty}$  are sufficiently involved that they merit separate discussion. This algorithm assumes that the orbital characteristics  $E$ ,  $L_z$ ,  $Q$ , and  $r$  are known, as are the harmonic indices  $l$ ,  $m$ ,  $k$  (and hence the frequency  $\omega_{mk}$ ), and the spheroidal harmonic expansion coefficients  $b_j^{a\omega}$ .

1. Integrate the Sasaki-Nakamura equation (4.19) inwards from “infinity” to  $r$  using Bulirsch-Stoer integration (as implemented in the routine `bsstep()` driven by `odeint()` from [47], modified to integrate complex functions of real arguments) to get  $X_{lmk}^\infty$ . This integration is done in Boyer-Lindquist coordinates. The value at “infinity” is set using the asymptotic form Eq. (4.21). It is of course impossible to actually integrate numerically from  $r = \infty$ , so we have implemented a variant of Richardson extrapolation [47] to accurately compute the value of  $X_{lmk}^\infty$ . Let  $r_i^\infty$  be the  $i$ th “big number” which will be used to approximate infinity, and let  $X_{i;lmk}^\infty$  be the value of  $X_{lmk}^\infty$  computed using  $r_i^\infty$  to set the  $r \rightarrow \infty$  boundary condition. We set  $r_1^\infty \simeq 30/\omega_{mk}$ , *i.e.*, roughly 5 mode wavelengths, and set  $r_{i+1}^\infty = 2 \times r_i^\infty$ . We then construct a rational function approximation to the sequence  $X_{i;lmk}^\infty$  as a function of  $x_i = 1/r_i^\infty$ , and use the approximation to extrapolate to the limit  $x = 0$ . We iterate until the difference in successive approximations is  $\sim 10^{-7}$ ; this typically requires 5 – 10 iterations. We have found this to be far more accurate and faster than simply setting “ $\infty =$  very large number” in the code.
2. Integrate the Sasaki-Nakamura equation from the event horizon to  $r$  to get  $X_{lmk}^H$ , using the asymptotic form Eq. (4.20) to set the value at the horizon. We use essentially the same numerical tricks and techniques as are used for  $X_{lmk}^\infty$ . In particular, we construct a rational function approximation to a sequence of values  $X_{i;lmk}^H$  computed using  $r_i^H = r_+ + x_i$ , where  $x_1 \sim 10^{-6}$  and  $x_{i+1} = x_i/2$ , and then extrapolate to  $x = 0$ . (This trick is needed since the Sasaki-Nakamura equation is not well-behaved in Boyer-Lindquist coordinates at the horizon.) Roughly 4 – 8 iterations are needed to get a result accurate to  $\sim 10^{-7}$ .
3. Integrate the Sasaki-Nakamura equation from  $r$  to infinity, using  $X_{lmk}^H$  as the value at  $r$ , and thereby compute the coefficient  $A_{lmk}^{\text{in}}$ . The same numerical techniques used to calculate  $X_{lmk}^\infty$  are used here to integrate the equation and to reach infinity.
4. Compute the homogeneous Teukolsky solutions  $R_{lmk}^{H,\infty}$  using Eq. (4.24), and  $B_{lmk}^{\text{in}}$  using Eq. (4.25a).
5. Compute  $Z_{lmk}^{H,\infty}$  using Eqs. (4.49) and (4.50).

This algorithm is then called by the “driver” algorithm for the step at which  $Z_{lmk}^{H,\infty}$  are needed.

## B. Code validation

In order to verify that the algorithms described in Sec. V A are working reliably, we ran a series of tests to make sure that the code reproduces known results in the proper limits. First, we analyzed the weak-field limit and verified that the code reproduces the results given in [32] (who analyzed gravitational radiation emitted by point particles orbiting black holes using a post-Newtonian expansion). Second, we took the limit  $a = 0$  and verified that the radiation emitted by a particle in an inclined orbit about a Schwarzschild black hole has the correct behavior.

Appendices G and I of [32] give (very long and detailed) post-Newtonian expansions of the energy flux to infinity and down the horizon for a particle orbiting in the equatorial plane of a Kerr black hole. These formulae allow us to check that the fluxes at infinity and down the horizon agree with known results as a function of the orbit’s radius  $r$  and the black hole’s spin  $a$ . We have compared both fluxes for a large number of cases and found excellent agreement (to the degree expected) for all parameters. Figure 1 is a typical example, comparing for  $l = 3$  the numerically computed downhole flux for a co-rotating orbit at  $r = 25M$  as a function of black hole spin  $a$ . The fits are quite good (except for  $l = 3, m = 2$ ) even in this relatively strong-field region because in most cases the post-Newtonian expansion formulae of [32] are very robust, including many powers of  $M/r$ . (There are not as many terms given for the case  $l = 3, m = 2$ , so the fits are not as robust in that case.)

These tests demonstrate the code reliably produces radiation in the Kerr equatorial plane. The next check was whether the code reliably produces radiation for orbits out of the equatorial plane. A simple test is to examine inclined orbits in the Schwarzschild limit. In this limit, the *total* flux radiated for a given  $l$  mode must be invariant as the plane of the orbit is tilted (due to spherical symmetry); however, the *distribution* of the radiation among the  $k$  and  $m$  indices changes. The nature of this change can be deduced by examining the Teukolsky equation source, Eq. (4.26). In the Schwarzschild limit, the spin-weighted spheroidal harmonic  ${}_{-2}S_{lm}^{a\omega}(\theta)$  reduces to a spin-weighted spherical harmonic  ${}_{-2}Y_{lm}(\theta)$  (cf. Appendix A 2). The behavior of the system under rotation follows from the behavior of  ${}_{-2}Y_{lm}(\theta)$  under rotation.

The rotation behavior of *zero*-weight spherical harmonics (*i.e.*, the usual well-loved spherical harmonic) is well understood: if one rotates about the  $x$ -axis of the coordinate system (so that the  $\phi$  angles remain unchanged) by some angle  $\iota$ , then spherical harmonics in the new (primed) coordinate system are related to those in the original (unprimed) coordinate system via

$${}_0Y_{lm}(\theta') = \sum_{m'=-l}^l \mathcal{D}_{m'm}^l(\iota) {}_0Y_{lm'}(\theta). \quad (5.3)$$

The function  $\mathcal{D}_{m'm}^l(\iota)$  is the Wigner D-function; an explicit expression for it is given in Eqs. (4.255)–(4.256) of [48] (with Arfken’s angles  $\alpha$  and  $\gamma$  set to zero, and  $\beta = \iota$ ). It represents one element of a matrix that rotates spherical harmonics. Because this matrix commutes with the differential operator  $\partial$  which lowers the spin weights of spherical harmonics (cf. Appendix A 2), Eq. (5.3) applies to *any* spin weight.

From this, it is a simple matter to show that the energy emitted by a particle orbiting at angle  $\iota$  into some set of harmonic indices  $(l, m, k)$  is related to that emitted into the indices  $(l, m)$  by a particle in equatorial orbit by

$$\frac{\dot{E}_{lmk}(\iota)}{\dot{E}_{lm}^{\text{eq}}} = |\mathcal{D}_{(k-m),m}^l(\iota)|^2. \quad (5.4)$$

We have rather exhaustively compared the right- and left-hand sides of Eq. (5.4). In Figure 2, we show a typical comparison,  $l = 4$ ,  $m = 2$ ,  $k = 1$ . The numerical points agree with the analytic D-function curve to a fractional error  $\sim 10^{-6} - 10^{-7}$ ; this kind of agreement was found in all cases examined. This indicates that the off-equator capabilities of the code should be reliable.

In addition to these tests, we compared this code with unpublished results from D. Kennefick (whose code was used for the analysis of [35]) and L. S. Finn (whose code is used for the analysis of [7]). These two codes generate radiation for equatorial Kerr orbits. In all cases, we have found very good agreement (typically agreeing to the number of digits available with Finn’s code, and fractional error  $10^{-5} - 10^{-6}$  compared to Kennefick’s code). This, plus the validation tests described above, give us great confidence that the results found with this code are reliable.

## VI. RESULTS

The major results of this analysis break into two pieces: the gravitational waves (and associated energy spectra) produced by particular orbits, and the sequence of orbits through which the system passes as it evolves due to radiation reaction. We consider these results separately below.

### A. Radiation emitted at particular orbits

These results were computed by implementing the algorithm discussed in Sec. V A, using the value  $\epsilon_k = 10^{-7}$  (so that  $\epsilon_l = 10^{-6}$ ). The waveforms should therefore have a fractional accuracy of about  $10^{-5} - 10^{-6}$ . We discuss in detail two particular strong-field orbits.

1.  $r = 7M$ ,  $a = 0.95M$ ,  $\iota = 62.43^\circ$

The gravitational waveform produced by this orbit is shown in Figure 3. To achieve fractional accuracy  $10^{-6}$  on the  $l$ -loop required summing to  $l = 12$ . For each value of  $l$ , there are of course  $2l + 1$  values of  $m$ ; and for each value of  $m$ , we needed to compute 4 to 20 values of  $k$  to achieve fractional accuracy  $10^{-7}$  on the  $k$ -loop. The code uses roughly 2800 separate harmonics for this orbit. The fundamental orbital frequencies have values  $M\Omega_\phi = 0.05424$ ,  $M\Omega_\theta = 0.04954$ .

A notable feature of this waveform is the presence of many short timescale features (*e.g.*, the small bump in  $h_+$  near  $t = 300M$ , and the spiky features in  $h_\times$  between  $t = 1100M$  and  $t = 1500M$ ). The presence of these features is consistent with the breadth of this orbit’s energy spectrum with respect to  $k$  (cf. Fig. 4). High frequencies play a rather important role in determining the radiation to infinity because the Teukolsky potential [Eq. (4.3)] is rather transmissive to high frequency modes for large  $a$  [22]. Thus, many sum and difference harmonics of the fundamental frequencies are needed to accurately describe the motion. The low-frequency modulation of the waveform is due to frame-dragging induced precession of the orbital plane — Lense-Thirring precession.

The downhole energy spectrum for this orbit is plotted in Fig. 5. The most notable feature is that the energy radiated “down the hole” is negative: rather than the orbit losing energy down the horizon, this indicates that the orbit gains energy *from* the hole. This seemingly bizarre phenomenon is due to superradiant scattering [46]: the radiation extracts energy from the ergosphere of the Kerr black hole and pumps that energy into the orbit. This

transfers energy from the black hole’s spin to the particle’s orbit, slowing the inspiral. It is essentially a manifestation of the Penrose process.

Calculations such as this have excited interest in the past in the possibility of “floating orbits” [50]: orbits which absorb exactly as much energy as they lose to infinity, stopping their secular inspiral due to radiation loss [51]. Floating orbits would appear to be incredibly interesting objects: as sources of gravitational radiation, they would produce strong-field, nearly stationary signals, offering the possibility of very high precision studies of the Kerr ergosphere and the strong-field spacetime of black holes. Working with D. Kennefick, and checking all results with his code [35], we have examined very strong-field circular equatorial orbits of nearly maximal Kerr black holes (for which superradiance is strongest, and so are most likely to have floating orbits). We find that in no cases does the energy “flowing out of the horizon” come close to that radiated to infinity: summing over all multipoles, we find that at best  $\dot{E}^H \sim -0.1 \dot{E}^\infty$ . Although we could not find this result in the published literature, other authors who have written similar codes (S. Detweiler and L. S. Finn in particular) have come to the same conclusion [52].

Table I shows summed radiation reaction quantities for this orbit. They are compared with the values computed from the post-Newtonian approximation, using formulae due to Ryan [38]. These numbers, coupled with the numbers for orbits at  $r = 7M$ ,  $a = 0.05M$  (cf. Sec. VI A 2 and Table II) indicate that the post-Newtonian formulae are not particularly useful in the strong-field. As predicted by Ryan, our results indicate that the inclination angle increases — the orbit tends to evolve toward anti-alignment with the black hole’s spin. However, the quantitative details of the post-Newtonian predictions are rather inaccurate. In particular, they underestimate the rate at which the radius changes (by about a factor of two in this case) and overestimate the rate at which the inclination angle changes (in this case, by a factor of three). (Interestingly, this table shows that the post-Newtonian predictions for  $\dot{L}_z$  and  $\dot{E}$  aren’t nearly as inaccurate as for  $\dot{r}$  and  $\dot{i}$ . Small errors in  $\dot{L}_z$  and  $\dot{E}$  tend to magnify to large errors in  $\dot{r}$  and  $\dot{i}$ .)

$$2. \quad r = 7M, \quad a = 0.05M, \quad \iota = 60.17^\circ$$

The gravitational waveform produced in this case is shown in Fig. 6. Fractional accuracy of  $10^{-6}$  on the  $l$ -loop here required summing to  $l = 10$ . As in the case  $a = 0.95M$ , the code needed 4 to 20 values of  $k$  for fractional accuracy  $10^{-7}$  on the  $k$ -loop. In this case, the code needed roughly 1300 harmonics. The fundamental orbital frequencies have values  $M\Omega_\phi = 0.05407$ ,  $M\Omega_\theta = 0.05378$ .

Two features of this waveform are noteworthy, especially in comparison with the waveform in Fig. 3. First, note that the low-frequency modulation of the waveform is much slower. This is because the dragging of inertial frames is so much slower — the modulation is caused by the plane of the particle’s orbit precessing about the black hole. At least at lowest order, this Lense-Thirring precession frequency is proportional to the black hole’s spin. Second, it is clear that the waveform is much “simpler” for small spin: far fewer short timescale features are present (see the lowest panel of Fig. 6). This is reflected in the narrowness of the spectra of energy radiated to infinity (Fig. 7). When the black hole’s spin is small, the Teukolsky potential is not particularly transmissive to high-frequency radiation; a large number of sum and difference harmonics aren’t needed. The radiation at infinity is largely determined by radiation emitted at frequencies  $\omega \simeq 2\Omega_\phi$ ,  $\omega \simeq \Omega_\theta + \Omega_\phi$ , and  $\omega \simeq 2\Omega_\theta$ . (For small spins,  $\Omega_\phi \simeq \Omega_\theta$ , so these three frequencies are very nearly equal.)

The downhole energy spectrum is plotted in Fig. 8. Note that it is *nowhere* negative: for  $a = 0.05M$ , the particle does not extract any orbital energy from the black hole’s spin. The ergosphere for such a slowly rotating hole is small and unimportant, so radiation emitted toward the hole tends to be absorbed by the event horizon rather than being superradiantly scattered.

Table II gives the summed radiation reaction quantities, again comparing versus Ryan’s post-Newtonian results. As in the case  $a = 0.95M$ , we see that the post-Newtonian results give the qualitatively correct result (orbital radius shrinks and tilt increases), but are not quantitatively accurate in the strong field. Here, post-Newtonian theory underestimates the rate at which the orbital radius changes by a factor of roughly three, and overestimates the rate at which the inclination angle changes by about 50%.

The behavior of  $dE/dt$  summed over all  $l$  as a function of  $\omega$  is shown in Fig. 9. For both the downhole energy and energy radiated to infinity, the greatest radiated flux occurs at  $\omega \simeq 0.1/M \simeq 2\Omega_\phi \simeq 2\Omega_\theta$ . Peaks in the spectrum occur near all integer multiples of  $\Omega_\phi$  and  $\Omega_\theta$ . For  $a = 0.95M$ , these peaks are fairly broad. This is because there is power at many sum and difference harmonics of  $\Omega_\phi$  and  $\Omega_\theta$ . Since the fractional difference in these frequencies is about 10%, all power spikes are distinctly separated from one another. For  $a = 0.05M$ , these peaks are quite narrow. The fractional difference between  $\Omega_\phi$  and  $\Omega_\theta$  is only about 0.5% in this case, so spikes for the various sum and difference harmonics are *not* distinctly separated.

To demonstrate convergence to the post-Newtonian results, Tables III and IV show summed radiation reaction quantities for orbits at  $r = 100M$ , spins  $a = 0.95M$  and  $a = 0.05M$ , and inclination angles near  $60^\circ$ . The numerical



results are in much better agreement with the post-Newtonian results. This is not surprising, since  $r = 100M$  is a relatively weak-field region of the spacetime. It is however reassuring; these tables are further evidence that the code’s results are trustworthy.

## B. Radiation reaction sequences

Fig. 10 shows a section of the parameter space in the strong-field of a Kerr black hole with spin  $a = 0.8M$ . As discussed in the Introduction, this is a reasonable choice for supermassive black holes whose spin has been buffered by magnetohydrodynamic extraction of the holes’ spin energy [23–25]. Each  $(r, \iota)$  coordinate point in this figure represents an orbit. The dotted line separates stable from unstable orbits: orbits to the left of the curve are unstable to perturbations and catastrophically plunge into the black hole. [This line is calculated by solving the system  $R = R' = R'' = 0$  for the constants parameterizing marginally stable orbits, where  $R$  is defined in Eq. (2.1a).]

The effect of radiation reaction on these orbits is indicated in Fig. 10 by arrows at various points in the figure. The tail of each arrow indicates a particular orbit; the arrow itself is proportional to the vector  $[(M/\mu)\dot{r}, (M^2/\mu)\dot{\iota}]$ . The arrow points in the direction to which radiation reaction pushes the particle from orbit to orbit, and its length indicates how rapidly radiation reaction acts. As might be expected from the discussion in Sec. VI A, the arrows in this figure indicate that the inclination angle does not change very quickly. One can regard the arrows as representing tangent vectors to a radiation reaction trajectory  $[r(t), \iota(t)]$ . The nearly horizontal aspect of the arrows in this figure indicates that radiation reaction would change  $\iota$  by little during a physical inspiral.

The extremely long arrow near  $r = 7M$ ,  $\iota \simeq 120^\circ$  in Fig. 10 highlights the effect radiation reaction has on orbits which are close to the maximum inclination angle for stable orbits. That particular point is at  $\iota = 119.194^\circ$ ; the maximum inclination angle at  $r = 7M$  is  $\iota = 119.670^\circ$ . Because it is extremely close to the marginally stable orbit, a small “push” from radiation reaction has a very large effect. Orbits that are close to the stability threshold are quickly pushed into the hole by gravitational-wave emission.

Figure 11 plots  $i$  as a function of  $\iota$  for various black hole spins. All curves are for orbits at  $r = 10M$ . Notice that, for large spin, the distribution’s peak is pushed away from  $\iota = 90^\circ$ , where first order post-Newtonian analysis predicts  $i$  is maximal [cf. Eq. (3.9), which predicts  $i \propto \sin \iota$ ]. One can see that the post-Newtonian prediction is more accurate for small spin. This is not surprising, since Eq. (3.9) is based on leading order expansions in both  $M/r$  and  $a/M$ . Although not shown here, the peak moves toward  $90^\circ$  as  $r/M$  increases, indicating that this shift is truly a strong-field effect.

## VII. CONCLUSION

The results presented in this paper give the first strong-field radiation reaction results in which the Carter constant evolves in a non-trivial manner. Circular, non-equatorial orbits are probably, however, the only case in which one can evolve the Carter constant by examining radiation fluxes — in all other cases, Eq. (3.5), relating  $\dot{Q}$  to  $\dot{E}$  and  $\dot{L}_z$ , will not hold. More general prescriptions for evolving the Carter constant will require calculation of an instantaneous radiation reaction force. Because the results presented here are constrained to circular orbits, we cannot pretend that they are in any way generic. However, they contain some very interesting features that may carry over to more general — eccentric and inclined — orbits. They also should provide useful checks to future calculations that use a radiation reaction force.

The calculations presented here indicates that  $i$  is relatively small. In particular, they show that the (dimensionless) ratio  $Mi/\dot{r} \ll 1$ . If this result holds in general, it suggests an approximation in which one holds the inclination angle fixed and allows the radius and eccentricity to radiatively evolve [53]. Such an approximation might give a first cut of the trajectory a system follows through the phase space  $(r, e, \iota)$  of allowed orbits, perhaps serving as the first order solution to an iterative scheme for finding such trajectories to higher accuracy. (It is worth noting, though, that preliminary investigations of very strong-field orbits of rapidly rotating holes indicate that the inclination angle changes rather more dramatically. This result will be presented in a followup paper [27].)

The effect of spin on the gravitational waveforms (cf. the waves plotted in Figs. 3 and 6, and their associated emission spectra, Figs. 4 – 5 and 7 – 8) is marked: large spin causes many harmonics of the fundamental frequencies  $\Omega_\phi$  and  $\Omega_\theta$  to influence the waveform. This is reflected by the relative breadth of emission spectra. It seems likely that generic orbits — which will be further influenced by a third frequency,  $\Omega_r$  — will have this property as well, and we thus expect to see many harmonics of all three frequencies to influence the waveform in the general case. In terms of gravitational-wave observations, this impact of the spin parameter could be nice: with such a marked effect, the black hole’s spin might be measurable to high accuracy. On the other hand, because it has such a marked effect, data

analysis might require an unreasonably large number of waveform templates: waveforms that are very “interesting” (in the sense of having a rich, detailed structure) typically require many templates so that signal-to-noise is not lost in measurement. To understand how many templates are needed would require constructing accurate radiation reaction sequences through the phase space  $(r, \iota)$  [ $(r, e, \iota)$  in the general case], building the waveforms emitted along such sequences, and then constructing the metric on the manifold of waveform shapes as prescribed by Owen [54]. If the number of templates is very large, hierarchical search techniques will probably be needed. These analyses are beyond the scope of this paper [55].

Finally, the two central approximations that go into the calculations here — adiabaticity and averaging over all members of the orbit family — could have a large effect on gravitational waveforms, and hence on observations by space based detectors such as LISA. First, as noted in Eq. (3.16), the adiabatic assumption which goes into these calculations requires that the mass ratio be rather extreme in the strong field. Astrophysical high-mass-ratio systems of interest for gravitational-wave observations are likely to have  $\mu/M \sim 10^{-4} - 10^{-7}$ . This might not be extreme enough for astrophysical systems to evolve adiabatically into the strong-field regime. However, it is impossible to relax the adiabatic assumption without turning to an instantaneous radiation reaction force. Second, by averaging over all members of the orbit family, we wash away any influence of initial conditions on the radiation reaction sequence — the position and momentum of the orbiting particle when observations begin. This averages the characteristics of the “true” waveform over the time  $T_{\text{return}}$  it takes for the orbit to return (or at the very least, come very close to) its initial conditions. (“True” waveform means the waveform constructed by evolving along a radiation reaction sequence, not just the snapshots presented here at specific moments on the sequence.) For highly eccentric, inclined orbits, this time could turn out to be very long. If, in particular, it turns out to be longer than the time it takes for radiation reaction to change the system’s orbital characteristics, such averaging would not be at all accurate. In this case, templates constructed for the analysis of LISA-type gravitational-wave observations would require not only information about the trajectory through the orbital phase space  $(r, e, \iota)$  but also about the initial conditions of all possible orbits. This could drastically increase the number of needed templates.

In the end, we find that many of the questions raised here require the instantaneous radiation reaction force  $f_{\text{RR}}^\mu$ . Although “radiation reaction without radiation reaction force” analyses such as the one in this paper provide much insight and valuable information about the waveforms emitted by high-mass-ratio systems, they are essentially limited by the approximations that go into them, and cannot answer some of the most important questions. Because of the eminent need, driven by future gravitational-wave observations, to understand radiation reaction to very good accuracy in the high-mass-ratio limit, programs to compute the radiation reaction force should be given very high priority.

## ACKNOWLEDGMENTS

I am indebted to Daniel Kennefick for many useful conversations and assistance, as well as for helping to validate my results with his radiation reaction code; I likewise thank Sam Finn for providing data from his code to help validate my results. I am very grateful to Saul Teukolsky for suggesting the spectral decomposition technique for numerically calculating the spheroidal harmonics. For many fruitful conversations and advice, I particularly wish to thank those involved in the Capra Ranch Radiation Reaction Analysis Program: Lior Burko, Patrick Brady, Éanna Flanagan, Eric Poisson, and Alan Wiseman. Finally for many useful conversations I thank Roger Blandford, Curt Cutler, Steven Detweiler, Jeremy Heyl, Dustin Laurence, Yuri Levin, Sterl Phinney, Masaru Shibata, Hideyuki Tagoshi, and Kip Thorne. The package MATHEMATICA was used to aid some of the calculations; all of the numerical code was developed with tools from the Free Software Foundation. All plots were produced using the package SM. This research was supported at Caltech by NSF Grants AST-9731698 and AST-9618537, and NASA Grants NAG5-6840 and NAG5-7034; and at Illinois by NSF Grant AST-9618524.

## APPENDIX A: CALCULATION OF SPHEROIDAL HARMONICS

### 1. Spheroidal harmonics as a sum of spherical harmonics

The separated  $\theta$  dependence of the function  $\psi_4$  is governed by the equation

$$\frac{1}{\sin \theta} \frac{d}{d\theta} \left( \sin \theta \frac{d_s S_{lm}^{a\omega}}{d\theta} \right) + \left[ (a\omega)^2 \cos^2 \theta - 2a\omega s \cos \theta - \left( \frac{m^2 + 2ms \cos \theta + s^2}{\sin^2 \theta} \right) + \mathcal{E}_{lm} \right] {}_s S_{lm}^{a\omega} = 0. \quad (\text{A1})$$

For our purposes, we care only about the case  $s = -2$ . Solutions to this equation are the spin-weighted spheroidal harmonics. When  $a\omega = 0$ , the solutions are the spin-weighted spherical harmonics; in this case,  $\mathcal{E}_{lm} = l(l+1)$ .

This fact suggests that it may be useful to expand the spheroidal harmonics in spherical harmonics. This spectral decomposition takes the following form:

$${}_s S_{lm}^{a\omega}(\theta) = \sum_{j=l_{\min}}^{\infty} b_j^{a\omega} {}_s Y_{jm}(\theta) \quad (\text{A2})$$

Here, it is to be understood that  ${}_s Y_{lm}(\theta)$  denotes the spin-weighted spherical harmonics without including the  $\phi$  dependence:  ${}_s Y_{lm}^{\text{usual}}(\theta, \phi) = {}_s Y_{lm}(\theta) e^{im\phi}$ . Also,  $l_{\min} = \max(|s|, |m|)$ .

It is convenient at this point to adopt Dirac-style notation, so that

$$\begin{aligned} {}_s Y_{jm}(\theta) &\rightarrow |sjm\rangle, & {}_s \bar{Y}_{jm}(\theta) &\rightarrow \langle sjm|, \\ \int_0^\pi {}_s \bar{Y}_{lm}(\theta) f(\theta) {}_s Y_{jm}(\theta) \sin\theta d\theta &\rightarrow \langle slm|f(\theta)|sjm\rangle. \end{aligned} \quad (\text{A3})$$

Substitute Eq. (A2) into Eq. (A1), and use the fact that the functions  ${}_s Y_{jm}$  satisfy (A1) with  $a\omega = 0$  and  $\mathcal{E}_{jm} = j(j+1)$ . The result, in Dirac notation, is

$$\sum_{j=l_{\min}}^{\infty} b_j^{a\omega} [(a\omega)^2 \cos^2\theta - 2a\omega s \cos\theta - j(j+1)] |sjm\rangle = -\mathcal{E}_{lm} \sum_{j=l_{\min}}^{\infty} b_j^{a\omega} |sjm\rangle. \quad (\text{A4})$$

Next, multiply the above expression by  $\langle slm|$ . The various inner products are simply evaluated [56]:

$$\begin{aligned} \langle slm| \cos^2\theta |sjm\rangle &= \frac{1}{3}\delta_{jl} + \frac{2}{3}\sqrt{\frac{2l+1}{2j+1}} \langle j, 2, m, 0|l, m\rangle \langle j, 2, -s, 0|l, -s\rangle \equiv c_{j,l,2}^m, \\ \langle slm| \cos\theta |sjm\rangle &= \sqrt{\frac{2l+1}{2j+1}} \langle j, 1, m, 0|l, m\rangle \langle j, 1, -s, 0|l, -s\rangle \equiv c_{j,l,1}^m, \\ \langle slm|sjm\rangle &= \delta_{jl}. \end{aligned} \quad (\text{A5})$$

The numbers  $\langle j, i, m, 0|l, n\rangle$  are Clebsch-Gordan coefficients. The fact that Clebsch-Gordan coefficients appear in this expression greatly simplifies the sums: it tells us that  $c_{j,l,2}^m \neq 0$  only for  $j \in [l-2, l-1, l, l+1, l+2]$ , and  $c_{j,l,1}^m \neq 0$  only for  $j \in [l-1, l, l+1]$ . Performing the sums, we find

$$\begin{aligned} b_{l-2}^{a\omega} (a\omega)^2 c_{l-2,l,2}^m + b_{l-1}^{a\omega} [(a\omega)^2 c_{l-1,l,2}^m - 2a\omega s c_{l-1,l,1}^m] + b_l^{a\omega} [(a\omega)^2 c_{l,l,2}^m - 2a\omega s c_{l,l,1}^m - l(l+1)] \\ + b_{l+1}^{a\omega} [(a\omega)^2 c_{l+1,l,2}^m - 2a\omega s c_{l+1,l,1}^m] + b_{l+2}^{a\omega} (a\omega)^2 c_{l+2,l,2}^m = -\mathcal{E}_{lm} b_l^{a\omega}. \end{aligned} \quad (\text{A6})$$

Equation (A6) can be rewritten as a matrix equation, with the numbers  $b_l^{a\omega}$  representing the coefficients of the matrix's eigenvector, and  $\mathcal{E}_{lm}$  the matrix's eigenvalue. The matrix so defined is clearly band-diagonal, which means that solving for the eigenvalues and eigenvectors is rather simple. To do so, we used routines from [47].

## 2. Numerical calculation of spin-weighted spherical harmonics

The above section describes how to express the spin-weighted spheroidal harmonics as a sum of spin-weighted spherical harmonics; there remains the task of actually calculating the spherical harmonics. A favored method for stably and accurately calculating spherical harmonics of spin-weight zero is with a recurrence relation [47]. It is relatively simple to generalize such relations to stably and accurately calculate spherical harmonics of non-zero spin weight. Our discussion here will be relevant to calculation of spin weights 0, -1, and -2; generalization to other spin weights is straightforward. See [57] for further discussion.

To begin, we note that the operator  $\check{\partial}$  lowers the spin weight of a function as follows:

$$\begin{aligned} \check{\partial}_s Y_{lm}(\theta) &\equiv -(\sin\theta)^{-s} \left[ \frac{\partial}{\partial\theta} + \frac{m}{\sin\theta} \right] (\sin\theta)^s {}_s Y_{lm}(\theta) \\ &= -[(l+s)(l-s+1)]^{1/2} {}_{(s-1)} Y_{lm}(\theta). \end{aligned} \quad (\text{A7})$$

The plan is to apply  $\check{\partial}$  to  ${}_0Y_{lm}$  and derive formulae for the  ${}_{-1}Y_{lm}$ , and then to apply  $\check{\partial}$  to  ${}_{-1}Y_{lm}$  and derive formulae for the  ${}_{-2}Y_{lm}$ . Note also that there is an operator  $\hat{\partial}$  which raises the spin weight of a function:

$$\begin{aligned}\hat{\partial}_s Y_{lm}(\theta) &\equiv -(\sin \theta)^s \left[ \frac{\partial}{\partial \theta} - \frac{m}{\sin \theta} \right] (\sin \theta)^{-s} {}_s Y_{lm}(\theta) \\ &= [(l-s)(l+s+1)]^{1/2} {}_{(s+1)} Y_{lm}(\theta).\end{aligned}\tag{A8}$$

This operator will come in handy when computing derivatives of the spheroidal harmonics in Sec. A3 below.

The zero-weight spherical harmonics are written

$${}_0Y_{lm}(\theta) = A(l, m) P_{lm}(\cos \theta),\tag{A9}$$

where

$$A(l, m) = \sqrt{\frac{(2l+1)}{4\pi}} \sqrt{\frac{(l-m)!}{(l+m)!}},\tag{A10}$$

and the associated Legendre polynomial  $P_{lm}(x)$  can be accurately computed from the recurrence relation [47]

$$P_{lm}(x) = \frac{1}{l-m} [x(2l-1)P_{l-1,m} - (l+m-1)P_{l-2,m}]\tag{A11}$$

with starting values

$$\begin{aligned}P_{mm}(x) &= (-1)^m (2m-1)!! (1-x^2)^{m/2}, \\ P_{m+1,m}(x) &= x(2m+1)P_{mm}.\end{aligned}\tag{A12}$$

Now, operate on  ${}_0Y_{lm}$  with  $\check{\partial}$ . Combining Eqs. (A7) and (A9), and using the notation  $x \equiv \cos \theta$ , we see that

$${}_{-1}Y_{lm}(\theta) = -\frac{A(l, m)}{\sqrt{l(l+1)}} \left[ \sqrt{1-x^2} \frac{d}{dx} - \frac{m}{\sqrt{1-x^2}} \right] P_{lm}(x).\tag{A13}$$

We now need recurrence relations for the functions  $\sqrt{1-x^2} dP_{lm}/dx$  and  $P_{lm}/\sqrt{1-x^2}$ . (We treat these combinations as functions in and of themselves; this avoids problems as  $x \rightarrow \pm 1$ .) These relations are easily derived from Eqs. (A11) and (A12):

$$\begin{aligned}\frac{P_{lm}(x)}{\sqrt{1-x^2}} &= \frac{1}{l-m} \left[ x(2l-1) \frac{P_{l-1,m}}{\sqrt{1-x^2}} - (l+m-1) \frac{P_{l-2,m}}{\sqrt{1-x^2}} \right], \\ \frac{P_{mm}(x)}{\sqrt{1-x^2}} &= (-1)^m (2m-1)!! (1-x^2)^{(m-1)/2}, \\ \frac{P_{m+1,m}(x)}{\sqrt{1-x^2}} &= x(2m+1) \frac{P_{mm}}{\sqrt{1-x^2}};\end{aligned}\tag{A14}$$

$$\begin{aligned}\sqrt{1-x^2} \frac{dP_{lm}}{dx} &= \frac{1}{l-m} \left[ (2l-1) \left( \sqrt{1-x^2} P_{l-1,m} + x \sqrt{1-x^2} \frac{dP_{l-1,m}}{dx} \right) - (l+m-1) \sqrt{1-x^2} \frac{dP_{l-2,m}}{dx} \right], \\ \sqrt{1-x^2} \frac{dP_{mm}}{dx} &= -mx (-1)^m (2m-1)!! (1-x^2)^{(m-1)/2}, \\ \sqrt{1-x^2} \frac{dP_{m+1,m}}{dx} &= (2m+1) \left[ \sqrt{1-x^2} P_{mm} + x \sqrt{1-x^2} \frac{dP_{mm}}{dx} \right].\end{aligned}\tag{A15}$$

Next, operate on  ${}_{-1}Y_{lm}$  with  $\check{\partial}$ . Combine Eqs. (A7) and (A13) to obtain

$${}_{-2}Y_{lm}(\theta) = \frac{A(l, m)}{\sqrt{(l-1)l(l+1)(l+2)}} \left[ (1-x^2) \frac{d^2}{dx^2} - 2m \frac{d}{dx} + \frac{m^2 - 2mx}{1-x^2} \right] P_{lm}(x).\tag{A16}$$

For these harmonics, we need recurrence relations for  $P_{lm}/(1-x^2)$ ,  $dP_{lm}/dx$ , and  $(1-x^2)d^2P_{lm}/dx^2$ . Again, these are straightforwardly derived from Eqs. (A11) and (A12):

$$\begin{aligned}
\frac{P_{lm}(x)}{(1-x^2)} &= \frac{1}{l-m} \left[ x(2l-1) \frac{P_{l-1,m}}{(1-x^2)} - (l+m-1) \frac{P_{l-2,m}}{(1-x^2)} \right], \\
\frac{P_{mm}(x)}{(1-x^2)} &= (-1)^m (2m-1)!! (1-x^2)^{(m-2)/2}, \\
\frac{P_{m+1,m}(x)}{(1-x^2)} &= x(2m+1) \frac{P_{mm}}{(1-x^2)};
\end{aligned} \tag{A17}$$

$$\begin{aligned}
\frac{dP_{lm}}{dx} &= \frac{1}{l-m} \left[ (2l-1) \left( P_{l-1,m} + x \frac{dP_{l-1,m}}{dx} \right) - (l+m-1) \frac{dP_{l-2,m}}{dx} \right], \\
\frac{dP_{mm}}{dx} &= -mx(-1)^m (2m-1)!! (1-x^2)^{(m-2)/2}, \\
\frac{dP_{m+1,m}}{dx} &= (2m+1) \left[ P_{mm} + x \frac{dP_{mm}}{dx} \right];
\end{aligned} \tag{A18}$$

$$\begin{aligned}
(1-x^2) \frac{d^2 P_{lm}}{dx^2} &= \frac{1}{l-m} \left[ (2l-1) \left( 2(1-x^2) \frac{dP_{l-1,m}}{dx} + x(1-x^2) \frac{d^2 P_{l-1,m}}{dx^2} \right) - (l+m-1)(1-x^2) \frac{d^2 P_{l-2,m}}{dx^2} \right], \\
(1-x^2) \frac{d^2 P_{mm}}{dx^2} &= m(-1)^m (2m-1)!! (1-x^2)^{(m-2)/2} [x^2(m-2) - (1-x^2)], \\
(1-x^2) \frac{d^2 P_{m+1,m}}{dx^2} &= (2m+1) \left[ 2(1-x^2) \frac{dP_{mm}}{dx} + x(1-x^2) \frac{d^2 P_{mm}}{dx^2} \right].
\end{aligned} \tag{A19}$$

This procedure can be continued as far as one's stamina allows; we stop here since these functions are all that is needed for this paper.

### 3. Some derivatives of the spheroidal harmonics

In the source term  $\mathcal{T}_{lm\omega}$ , we encounter the terms  $L_2^\dagger S$  and  $L_1^\dagger L_2^\dagger S$  [where  $S$  is shorthand for  ${}_{-2}S_{lm}^{a\omega mk}(\theta)$ ]. Using the spectral decomposition described above, evaluating these derivatives is quite straightforward.

Consider first  $L_2^\dagger S$ . Using the spectral decomposition, this becomes

$$\begin{aligned}
L_2^\dagger S &= \sum_{k=l_{\min}}^{\infty} b_k L_{2-2}^\dagger Y_{km}(\theta) \\
&= \sum_{k=l_{\min}}^{\infty} b_k \left[ \partial_\theta - \frac{m}{\sin \theta} + 2 \cot \theta \right] {}_{-2}Y_{km}(\theta) + a\omega \sin \theta \sum_{k=l_{\min}}^{\infty} b_{k-2} Y_{km}(\theta).
\end{aligned} \tag{A20}$$

The operator that appears in the first term on the second line is  $-\hat{\partial}$  [cf. Eq. (A8)] for  $s = -2$ . Thus,

$$L_2^\dagger S = a\omega \sin \theta S - \sum_{k=l_{\min}}^{\infty} b_k [(k-1)(k+2)]^{1/2} {}_{-1}Y_{km}(\theta). \tag{A21}$$

Next consider  $L_1^\dagger L_2^\dagger S$ :

$$\begin{aligned}
L_1^\dagger L_2^\dagger S &= a\omega L_1^\dagger \sin \theta S - \sum_{k=l_{\min}}^{\infty} b_k [(k-1)(k+2)]^{1/2} L_{1-1}^\dagger Y_{km}(\theta), \\
&= a\omega \left[ \frac{\partial}{\partial \theta} - \frac{m}{\sin \theta} + \cot \theta + a\omega \sin \theta \right] \sin \theta S \\
&\quad - \sum_{k=l_{\min}}^{\infty} b_k [(k-1)(k+2)]^{1/2} \left[ \frac{\partial}{\partial \theta} - \frac{m}{\sin \theta} + \cot \theta + a\omega \sin \theta \right] {}_{-1}Y_{km}(\theta),
\end{aligned}$$

$$\begin{aligned}
&= a\omega \left\{ \sin^{-1} \theta \left[ \frac{\partial}{\partial \theta} - \frac{m}{\sin \theta} + a\omega \sin \theta \right] \sin \theta \right\} \sin \theta S \\
&\quad - \sum_{k=l_{\min}}^{\infty} b_k [(k-1)(k+2)]^{1/2} \left( \hat{\partial} + a\omega \sin \theta \right) {}_{-1}Y_{km}(\theta), \\
&= a\omega \sin \theta \left\{ \sin^{-2} \theta \left[ \frac{\partial}{\partial \theta} - \frac{m}{\sin \theta} + a\omega \sin \theta \right] \sin^2 \theta \right\} S \\
&\quad + \sum_{k=l_{\min}}^{\infty} b_k [(k-1)k(k+1)(k+2)]^{1/2} {}_0Y_{km}(\theta) - a\omega \sin \theta \sum_{k=l_{\min}}^{\infty} b_k [(k-1)(k+2)]^{1/2} {}_{-1}Y_{km}(\theta), \\
&= a\omega \sin \theta \left[ \frac{\partial}{\partial \theta} - \frac{m}{\sin \theta} + a\omega \sin \theta + 2 \cot \theta \right] S \\
&\quad + \sum_{k=l_{\min}}^{\infty} b_k [(k-1)k(k+1)(k+2)]^{1/2} {}_0Y_{km}(\theta) + a\omega \sin \theta L_2^\dagger S - (a\omega \sin \theta)^2 S. \tag{A22}
\end{aligned}$$

Thus, we finally end up with

$$L_1^\dagger L_2^\dagger S = \sum_{k=l_{\min}}^{\infty} b_k [(k-1)k(k+1)(k+2)]^{1/2} {}_0Y_{km}(\theta) + 2a\omega \sin \theta L_2^\dagger S - (a\omega \sin \theta)^2 S. \tag{A23}$$

Eqs. (A21) and (A23) are then used in the source term evaluation.

## APPENDIX B: FUNCTIONS THAT APPEAR IN THE SASAKI-NAKAMURA EQUATION

The function  $F(r)$  that appears in Eq. (4.19) is given by

$$F(r) = \frac{d\eta/dr}{\eta} \frac{\Delta}{r^2 + a^2}, \tag{B1}$$

where

$$\eta(r) = c_0 + c_1/r + c_2/r^2 + c_3/r^3 + c_4/r^4, \tag{B2}$$

and

$$\begin{aligned}
c_0 &= -12i\omega M + \lambda(\lambda + 2) - 12a\omega(a\omega - m), \\
c_1 &= 8ia[3a\omega - \lambda(a\omega - m)], \\
c_2 &= -24iaM(a\omega - m) + 12a^2[1 - 2(a\omega - m)^2], \\
c_3 &= 24ia^3(a\omega - m) - 24Ma^2, \\
c_4 &= 12a^4. \tag{B3}
\end{aligned}$$

The function  $U(r)$  that appears in Eq. (4.19) is given by

$$U(r) = \frac{\Delta U_1(r)}{(r^2 + a^2)^2} + G(r)^2 + \frac{\Delta dG/dr}{r^2 + a^2} - F(r)G(r), \tag{B4}$$

where

$$\begin{aligned}
G(r) &= -\frac{2(r-M)}{r^2 + a^2} + \frac{r\Delta}{(r^2 + a^2)^2}, \\
U_1(r) &= V(r) + \frac{\Delta^2}{\beta} \left[ \frac{d}{dr} \left( 2\alpha + \frac{d\beta/dr}{\Delta} \right) - \frac{d\eta/dr}{\eta} \left( \alpha + \frac{d\beta/dr}{\Delta} \right) \right], \\
\alpha &= -iK(r)\beta/\Delta^2 + 3idK/dr + \lambda + 6\Delta/r^2, \\
\beta &= 2\Delta[-iK(r) + r - M - 2\Delta/r]. \tag{B5}
\end{aligned}$$

The functions  $K(r)$  and  $V(r)$  are from the Teukolsky potential, Eq. (4.3).

- [1] See, *e.g.*, L. Blanchet, T. Damour, B. R. Iyer, C. M. Will, and A. G. Wiseman, Phys. Rev. Lett. **74**, 3515 (1995) and reference therein.
- [2] Examples of recent progress in numerical relativity for the binary black hole problem from the American Grand Challenge Alliance are: R. Gomez *et al.*, Phys. Rev. Lett. **80**, 3915 (1998); G. B. Cook *et al.*, Phys. Rev. Lett. **80**, 2512 (1998); A. M. Abrahams *et al.*, Phys. Rev. D **80**, 1812 (1998). Examples for matter sources are: K. Oohara and T. Nakamura, in *Relativistic Gravitation and Gravitational Radiation*, edited by J.-A. Marck and J.-P. Lasota (Cambridge University Press, Cambridge, 1997); N. T. Bishop *et al.*, Phys. Rev. D **60**, 024005 (1999); J. A. Font, M. Miller, W.-M. Suen, and M. Tobias, gr-qc/9811015; T. W. Baumgarte, S. A. Hughes, and S. L. Shapiro, Phys. Rev. D **60** 87501 (1999); M. Shibata, Phys. Rev. D, in press (gr-qc/9908027).
- [3] S. A. Teukolsky, Astrophys. J. **185**, 635 (1973).
- [4] K. Danzmann *et al.*, *LISA — Proposal for a Laser-Interferometric Gravitational Wave Detector in Space*, Max-Planck-Institut für Quantenoptik, Report MPQ 177 (1993); also K. Danzmann *et al.*, *LISA — Laser Interferometer Space Antenna, Pre-Phase A Report*, Max-Planck-Institut für Quantenoptik, Report MPQ 233 (1998).
- [5] S. Sigurdsson and M. J. Rees, Mon. Not. R. Astron. Soc. **284**, 318 (1997).
- [6] S. Sigurdsson, Class. Quantum Grav. **14**, 1425 (1997).
- [7] L. S. Finn and K. S. Thorne, in preparation.
- [8] Fintan D. Ryan, Phys. Rev. D **56**, 1845 (1997).
- [9] R. Narayan, R. Mahadevan, and E. Quataert, in *Theory of Black Hole Accretion Disks*, edited by M. A. Abramowicz, G. Bjornsson, and J. E. Pringle (Cambridge University Press, Cambridge, 1998).
- [10] R. Narayan, Ap. J., submitted; also astro-ph/9907328.
- [11] T. C. Quinn and R. M. Wald, Phys. Rev. D **56** 3381 (1997).
- [12] Y. Mino, M. Sasaki, and T. Tanaka, Phys. Rev. D **55**, 3457 (1997).
- [13] W. G. Anderson and E. E. Flanagan, in preparation.
- [14] A. G. Wiseman, in preparation.
- [15] A. Ori, Phys. Lett. A **202**, 347 (1995); A. Ori, Phys. Rev. D **55**, 3444 (1997). In these references, Ori gives a reasonable prescription for calculating the change in orbital quantities from a multipole decomposition, but does not take into account the need for regularization. Further work does take this into account [16].
- [16] L. Barack and A. Ori, Phys. Rev. D, submitted; also gr-qc/9912010.
- [17] A brief description of the approach described by Ori in [16] (specialized to the scalar interaction, and focusing on static charges) is given in an appendix of L. Burko, Class. Quantum Grav., in press (1999); also gr-qc/9911042.
- [18] L. Burko, in preparation; see also L. Burko, gr-qc/9911089.
- [19] C. W. Misner, K. S. Thorne, and J. A. Wheeler, *Gravitation* (Freeman, San Francisco, 1973), chapter 33.
- [20] R. A. Isaacson, Phys. Rev. **166**, 1272 (1968).
- [21] S. W. Hawking and J. B. Hartle, Commun. Math. Phys. **25**, 283 (1972).
- [22] S. Chandrasekhar, *The Mathematical Theory of Black Holes* (Oxford University Press, New York, 1983).
- [23] E. S. Phinney, private communication.
- [24] R. Moderski, M. Sikora, and J.-P. Lasota, Mon. Not. R. Astron. Soc. **301**, 142 (1998).
- [25] R. D. Blandford, private communication.
- [26] K. S. Thorne, Astrophys. J. **191**, 507 (1974).
- [27] S. A. Hughes, in preparation.
- [28] E. Poisson, Phys. Rev. D **47**, 1497 (1993).
- [29] C. Cutler, L. S. Finn, E. Poisson, and G. J. Sussman, Phys. Rev. D **47**, 1511 (1993).
- [30] T. Apostolatos, D. Kennefick, A. Ori, and E. Poisson, Phys. Rev. D **47**, 5376 (1993).
- [31] C. Cutler, D. Kennefick, and E. Poisson, Phys. Rev. D **50**, 3816 (1994).
- [32] Y. Mino, M. Sasaki, M. Shibata, H. Tagoshi, and T. Tanaka, Prog. Theor. Phys. Supplement No. 128 (1997).
- [33] S. L. Detweiler, Astrophys. J. **225**, 687 (1978).
- [34] M. Shibata, Phys. Rev. D **50**, 6297 (1994).
- [35] D. Kennefick, Phys. Rev. D **58**, 4012 (1998); also gr-qc/9805102.
- [36] D. C. Wilkins, Phys. Rev. D **5**, 814 (1972).
- [37] D. Kennefick and A. Ori, Phys. Rev. D **53**, 4319 (1996).
- [38] F. D. Ryan, Phys. Rev. D **53**, 3064 (1996).
- [39] Y. Mino, unpublished Ph.D. thesis, Kyoto University (1996).
- [40] M. Shibata, Prog. Theor. Phys. **90**, 595 (1993).
- [41] Shibata's analysis [40] only includes radiation to infinity. In this nearly spherically symmetric asymptotically-flat region, notions of  $L_x$  and  $L_y$  components to the angular momentum can be made rigorous. In the highly non-spherical region near the event horizon, such notions cannot be made rigorous. It would probably not be possible to generalize the notion of  $L_x$  and  $L_y$  to radiation carried down the event horizon.
- [42] M. Sasaki and T. Nakamura, Prog. Theor. Phys. **67**, 1788 (1982).
- [43] K. S. Thorne, R. H. Price, and D. A. MacDonald, *Black Holes: The Membrane Paradigm* (Yale University Press, New Haven, 1986), p. 38.

- [44] F. D. Ryan, Phys. Rev. D **52**, R3159 (1995).
- [45] D. Kennefick and A. Ori, Phys. Rev. D **53**, 4319 (1996).
- [46] S. A. Teukolsky and W. H. Press, Astrophys. J. **193**, 443 (1974).
- [47] W. H. Press, S. A. Teukolsky, W. T. Vetterling, and B. P. Flannery, *Numerical Recipes* (Cambridge University Press, Cambridge, 1992).
- [48] G. Arfken, *Mathematical Methods for Physicists* (Academic Press, Orlando, 1985), chapter 16.
- [49] R. A. Breuer, *Gravitational Perturbation Theory and Synchrotron Radiation*, Lecture Notes in Physics **44** (Springer-Verlag, Berlin, 1975).
- [50] W. H. Press and S. A. Teukolsky, Nature **238**, 211 (1972).
- [51] Any further evolution of the system would be driven by the spindown of the massive black hole as radiative energy losses bleed away its rotational energy. The timescale for a such a change would be extremely long, scaling as  $M^{-3}$ .
- [52] S. Detweiler, private communication; L. S. Finn, private communication (see also [7]).
- [53] This approximation was suggested by C. Cutler (C. Cutler, private communication).
- [54] B. J. Owen, Phys. Rev. D **53**, 6749 (1996).
- [55] Strictly speaking, the overlap between any two waveforms with different parameters presented in this paper is *zero*. This is because the waveforms last for infinite time and have strictly different frequencies. It is only when the waveforms are computed from a radiation reaction sequence that they last for finite time, and overlap with each other's frequency domains.
- [56] W. B. Campbell and T. Morgan, Physica **53**, 264 (1971).
- [57] J. N. Goldberg *et al.*, J. Math. Phys. **8**, 2155 (1967).



TABLE I. Comparison of certain orbital quantities computed numerically and computed using post-Newtonian expansions for orbits with  $r = 7M$ ,  $a = 0.95M$ ,  $\iota = 62.43^\circ$ . In this strong-field region, we do not expect post-Newtonian expressions to be particularly valid. Post-Newtonian theory underestimates  $\dot{r}$  by about 2, and overestimates  $i$  by about 3.

Orbital quantity	Numerical value	Post-Newtonian value
$(M/\mu)^2 \dot{E}$	$-3.3885 \times 10^{-4}$	$-3.2580 \times 10^{-4}$
$(M/\mu^2) \dot{L}_z$	$-3.3207 \times 10^{-3}$	$-3.5926 \times 10^{-3}$
$(M/\mu) \dot{r}$	$-4.6574 \times 10^{-2}$	$-2.7499 \times 10^{-2}$
$(M^2/\mu) i$	$1.2073 \times 10^{-4}$	$3.0806 \times 10^{-4}$

TABLE II. Comparison of certain orbital quantities computed numerically and computed using post-Newtonian expansions for orbits with  $r = 7M$ ,  $a = 0.05M$ ,  $\iota = 60.17^\circ$ . As in the  $a = 0.95M$  case, we do not expect post-Newtonian expressions to work well here in the strong-field. Post-Newtonian theory underestimates  $\dot{r}$  by about 3, and overestimates  $i$  by about 50%.

Orbital quantity	Numerical value	Post-Newtonian value
$(M/\mu)^2 \dot{E}$	$-3.9524 \times 10^{-4}$	$-3.7768 \times 10^{-4}$
$(M/\mu^2) \dot{L}_z$	$-3.6794 \times 10^{-3}$	$-3.5210 \times 10^{-3}$
$(M/\mu) \dot{r}$	$-1.0964 \times 10^{-1}$	$-3.6762 \times 10^{-2}$
$(M^2/\mu) i$	$1.0875 \times 10^{-5}$	$1.5867 \times 10^{-5}$

TABLE III. Comparison of certain orbital quantities computed numerically and computed using post-Newtonian expansions for orbits with  $r = 100M$ ,  $a = 0.95M$ ,  $\iota = 60.05^\circ$ . In this relatively weak-field regime, we expect to see much better agreement with post-Newtonian results. The numbers in this table bear out this expectation.

Orbital quantity	Numerical value	Post-Newtonian value
$(M/\mu)^2 \dot{E}$	$-6.2194 \times 10^{-10}$	$-6.3815 \times 10^{-10}$
$(M/\mu^2) \dot{L}_z$	$-3.1175 \times 10^{-7}$	$-3.1995 \times 10^{-7}$
$(M/\mu) \dot{r}$	$-1.2610 \times 10^{-5}$	$-1.2733 \times 10^{-5}$
$(M^2/\mu) i$	$1.2040 \times 10^{-10}$	$1.3389 \times 10^{-10}$

TABLE IV. Comparison of certain orbital quantities computed numerically and computed using post-Newtonian expansions for orbits with  $r = 100M$ ,  $a = 0.05M$ ,  $\iota = 60.00^\circ$ . As with the orbit at  $r = 100M$ ,  $a = 0.95M$ , we find much better agreement with post-Newtonian results.

Orbital quantity	Numerical value	Post-Newtonian value
$(M/\mu)^2 \dot{E}$	$-6.2372 \times 10^{-10}$	$-6.3990 \times 10^{-10}$
$(M/\mu^2) \dot{L}_z$	$-3.1191 \times 10^{-7}$	$-3.2000 \times 10^{-7}$
$(M/\mu) \dot{r}$	$-1.2676 \times 10^{-5}$	$-1.2797 \times 10^{-5}$
$(M^2/\mu) i$	$6.6936 \times 10^{-12}$	$7.0439 \times 10^{-12}$

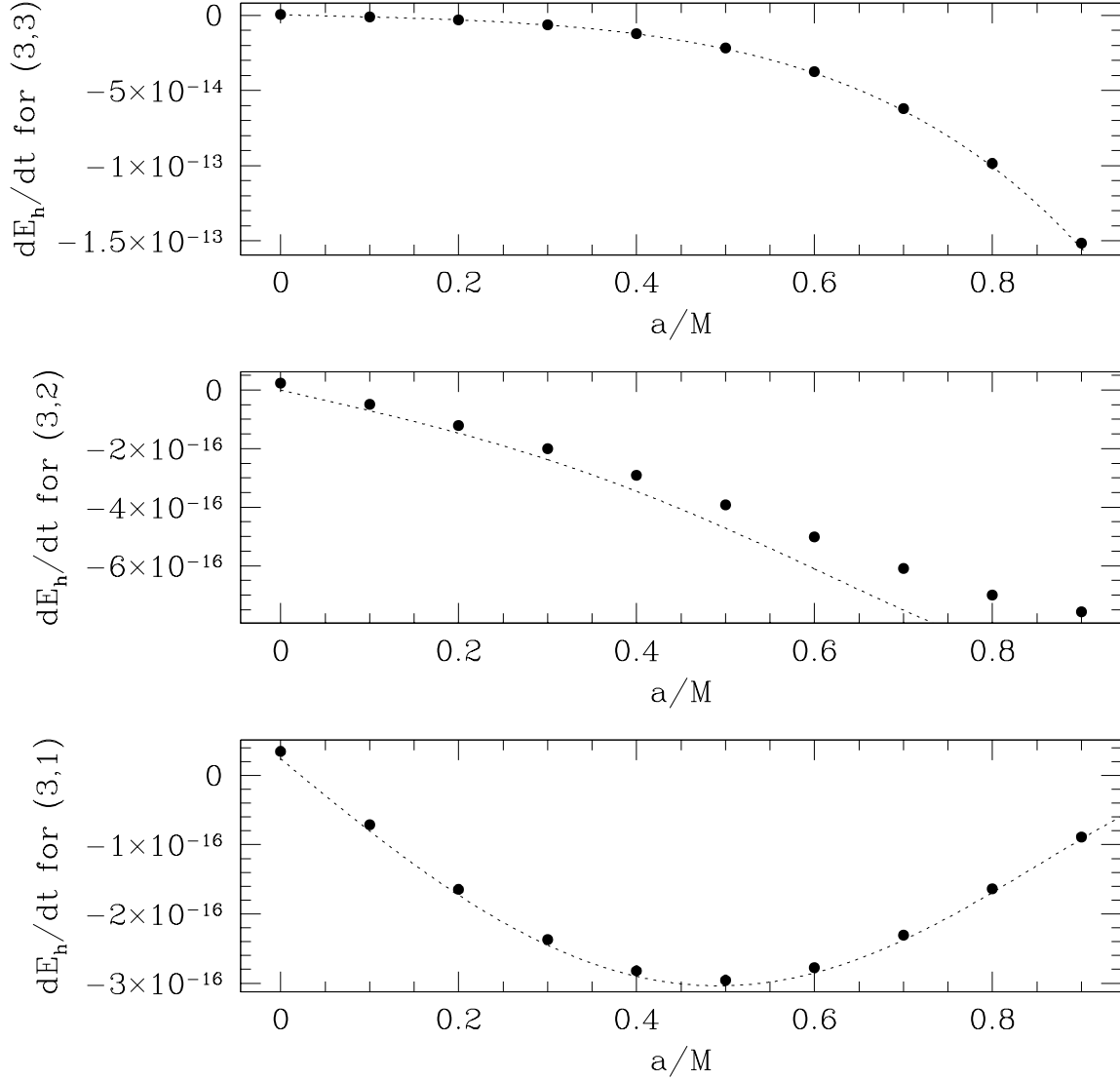


FIG. 1. Comparison of the flux down the event horizon for orbits at  $r = 25M$  as a function of black hole spin  $a/M$  for  $l = 3$  modes. Agreement between the numerical and post-Newtonian fluxes is quite good, except for  $m = 2$ ; this is because the post-Newtonian expansions contain many terms, and usually are quite robust. The case  $m = 2$  is an example where the expansion is not as robust. The interesting upturn in the down-horizon flux for  $m = 1$  and  $a \geq 0.5M$  is due to superradiant scattering — some incoming radiation gets scattered by the black hole’s ergosphere out to infinity.

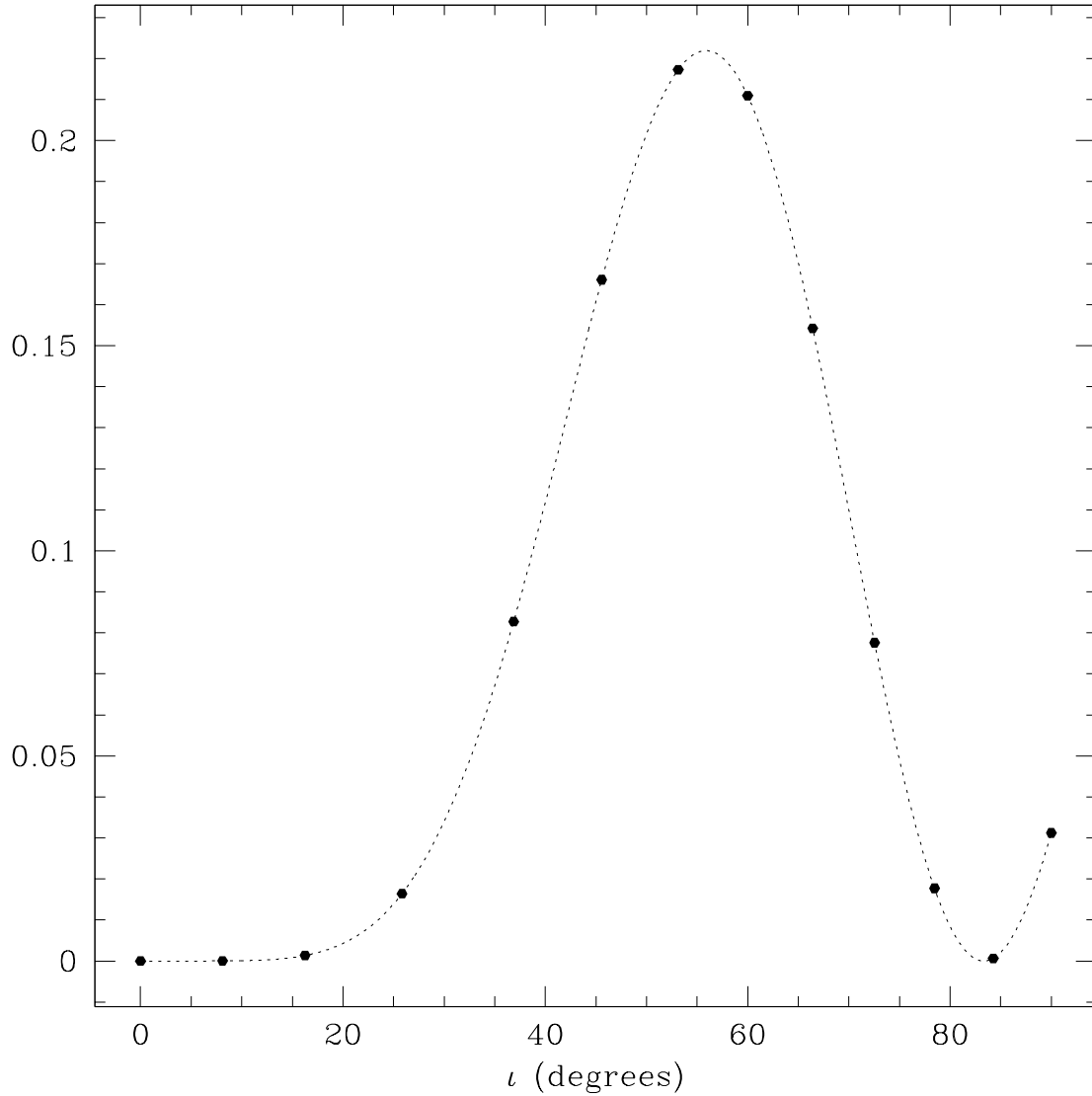


FIG. 2. Typical result of validation test for inclined, Schwarzschild orbits. The dotted line is the modulus squared of the Wigner D-function for  $l = 4$ ,  $m = 2$ ,  $k = 1$  as a function of inclination angle  $\iota$ ; the large black points are the ratio  $\dot{E}_{lmk}(\iota)/\dot{E}_{lm}^{\text{eq}}$ . The numerical data for the fluxes agrees with the analytical formula for the D-function to within  $10^{-6} - 10^{-7}$ . (For this plot, the numerical fluxes are evaluated at infinity; the results are identical to within the error when examining fluxes down the horizon. Also, these results are invariant — within the error bounds — as a function of orbital radius; this plot is generated for a particle orbiting at  $r = 15M$ .)

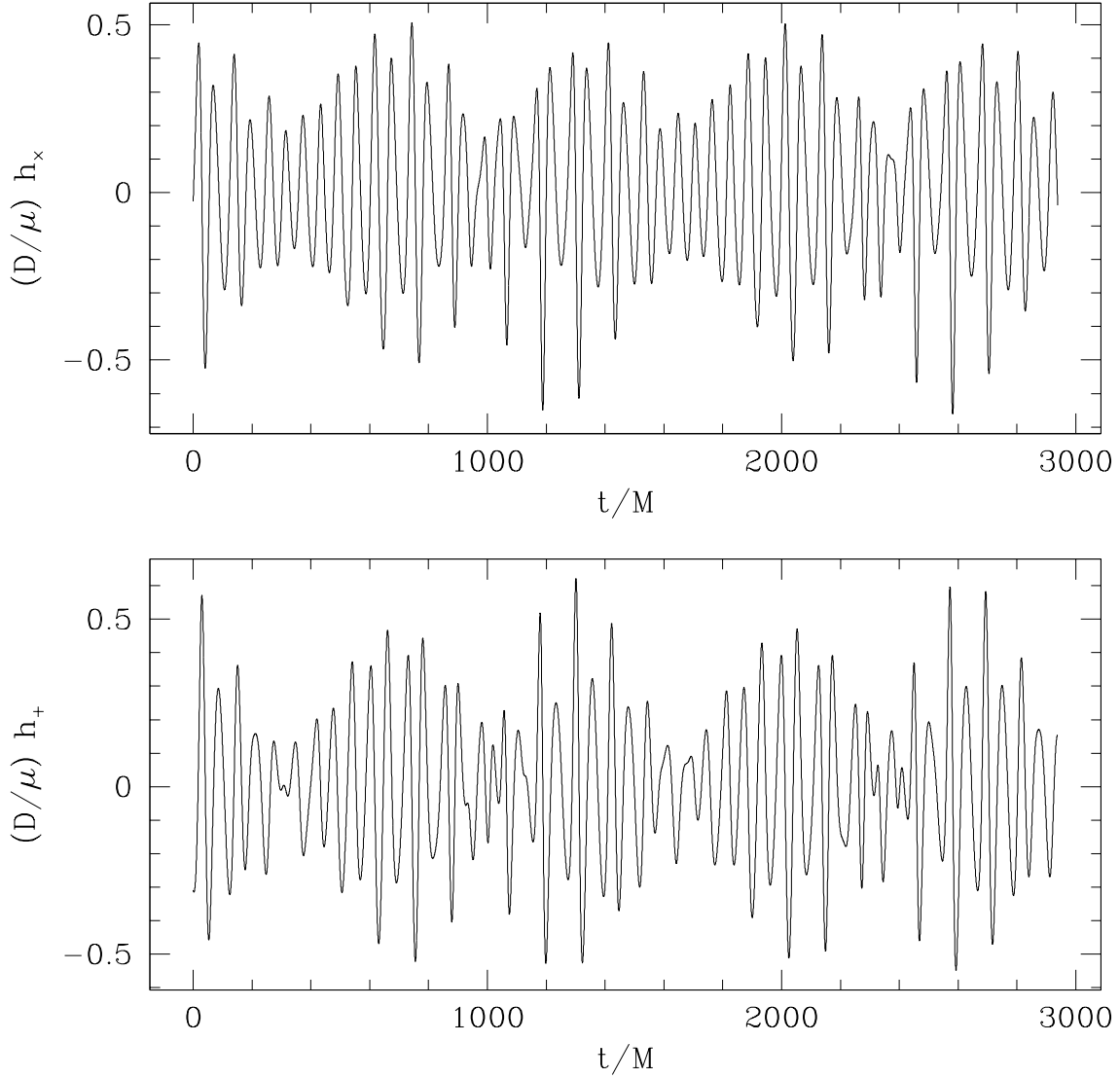


FIG. 3. The gravitational waveform produced by orbits with  $r = 7M$ ,  $\iota = 62.43^\circ$  about a black hole with  $a = 0.95M$ . The observer is in the hole's equatorial plane,  $\theta = 90^\circ$ . The distance to the source is  $D$ . Notice that there are many sharp features in this waveform, indicating the strong presence of relatively large harmonics of the fundamental frequencies  $\Omega_\phi$  and  $\Omega_\theta$ . This is consistent with the rather broad emission spectra produced by this orbit (cf. Fig. 4). The low frequency modulation is due to Lense-Thirring precession (*i.e.*, the precession of the orbital plane due to dragging of inertial frames by the black hole's spin).

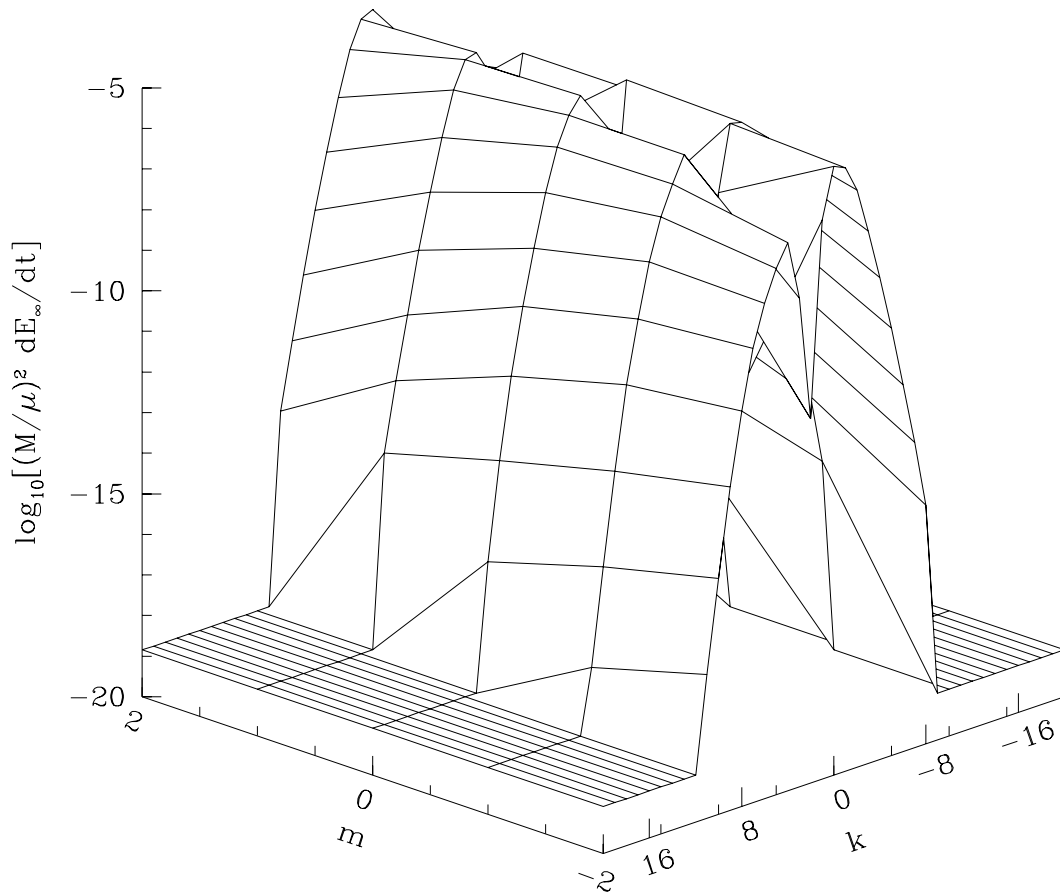


FIG. 4. The spectrum of energy for  $l = 2$  modes radiated to infinity by orbits with  $r = 7M$ ,  $\iota = 62.43^\circ$  about a black hole with  $a = 0.95M$ . Of particular note in this case is that the distribution is rather broad with respect to  $k$ . This is primarily due to the fact that for very large spin, the Teukolsky potential [cf. Eq. (4.3)] is fairly transmissive to high frequency modes. Notice that it is more transmissive to corotating modes ( $m\omega > 0$ ) than it is to counterrotating modes: corotating modes are more readily scattered by the hole.

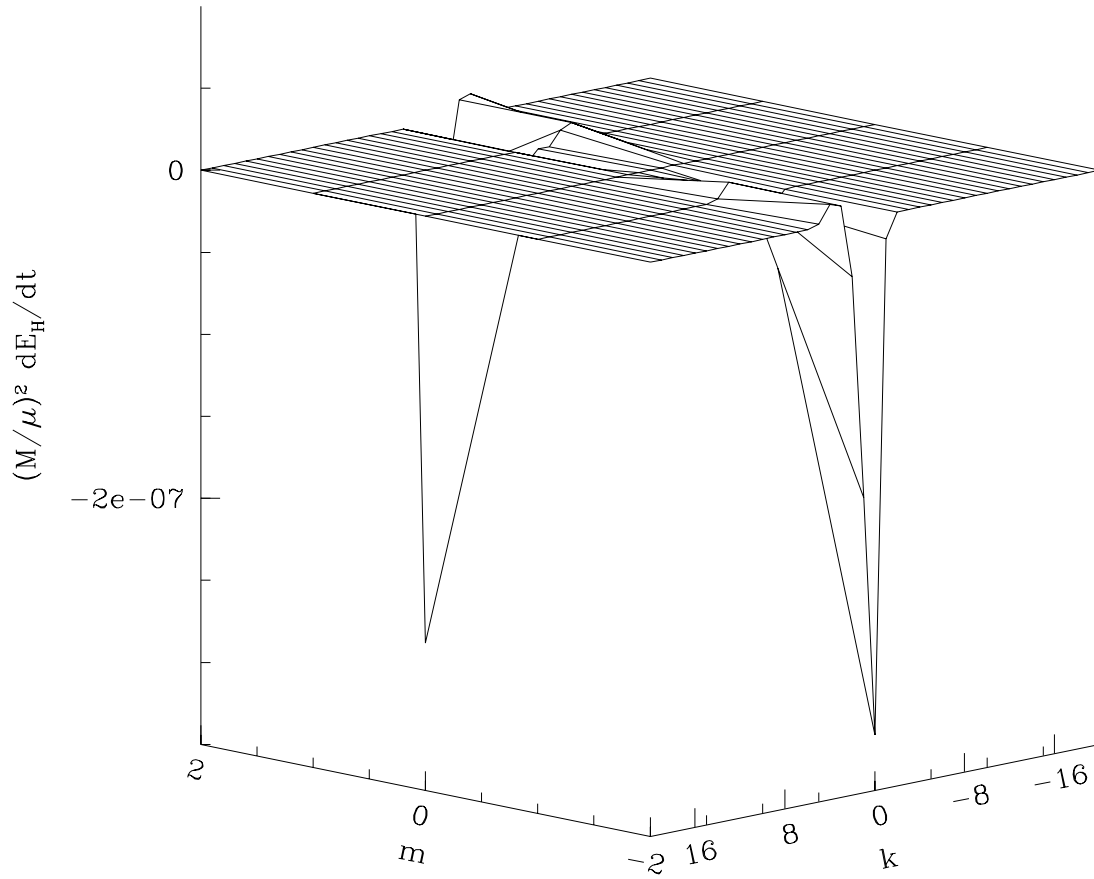


FIG. 5. The spectrum of energy radiated down the event horizon for  $l = 2$  modes for orbits with  $r = 7M$ ,  $\iota = 62.43^\circ$  about a black hole with  $a = 0.95M$ . The distribution is, for the most part, sharply negative (particularly for corotating modes,  $m\omega > 0$ ), indicating superradiant scattering. This is essentially a manifestation of the Penrose process — radiation extracts energy from the black hole's ergosphere.

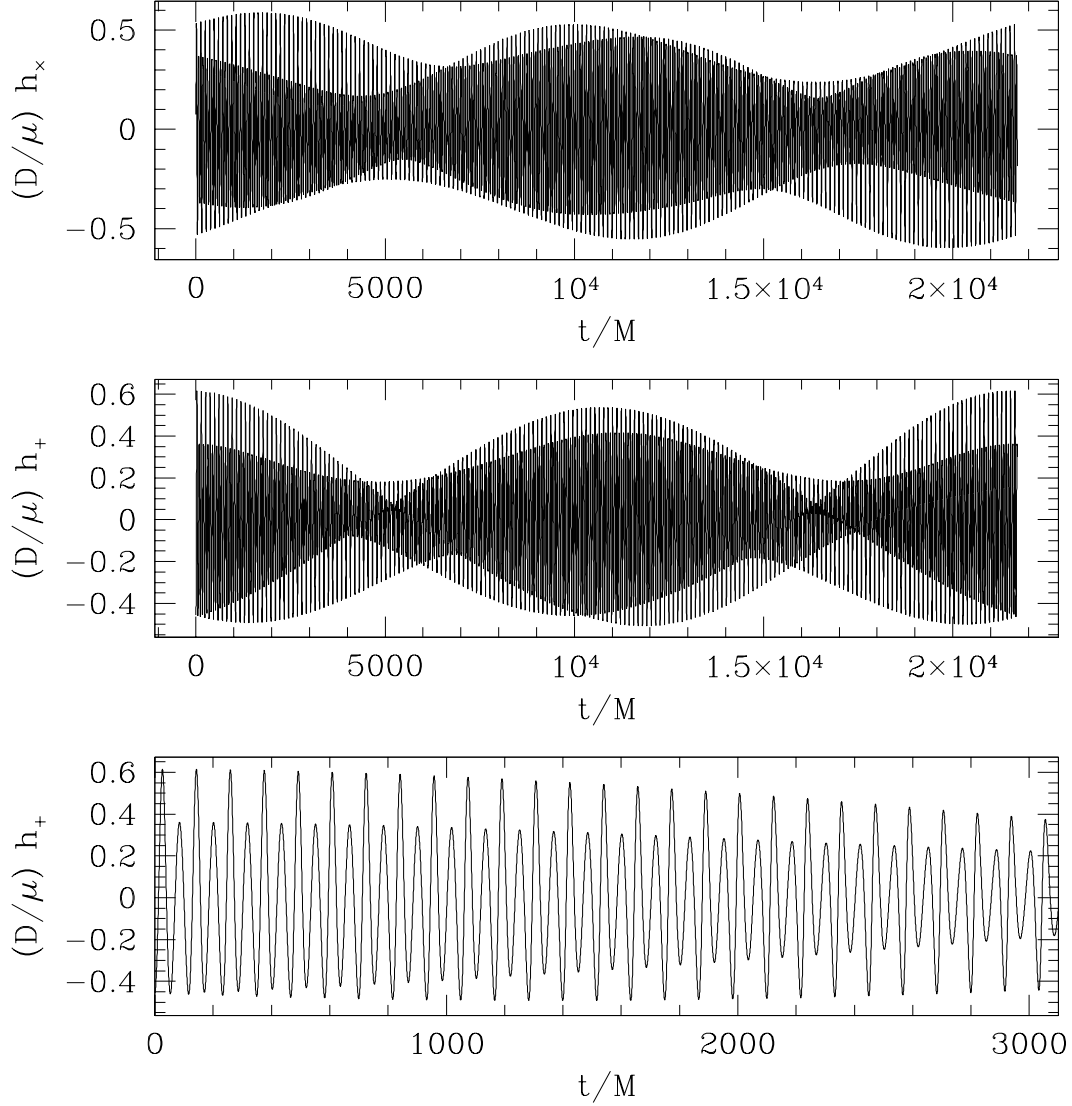


FIG. 6. The gravitational waveform produced by orbits with  $r = 7M$ ,  $\iota = 60.14^\circ$  about a black hole with  $a = 0.05M$ . The observer is in the hole's equatorial plane,  $\theta = 90^\circ$ . Although not much detail regarding the waveform is visible in this figure, the low frequency modulation is markedly slower than in the case  $a = 0.95$  (cf. Fig. 3). This is not surprising: the Lense-Thirring precession frequency is much smaller in this case since the spin is so low. The lowest panel is a zoom on  $h_+$ . The time shown is chosen so that comparison can be easily made with the waveform for  $a = 0.95M$ , Fig. 3. In contrast to the  $a = 0.95M$  case, the waveform is quite a bit simpler, lacking the many sharp features seen when there is large spin. This is primarily because the Teukolsky potential (4.3) is not nearly as transmissive to high-frequency modes when  $a$  is small.

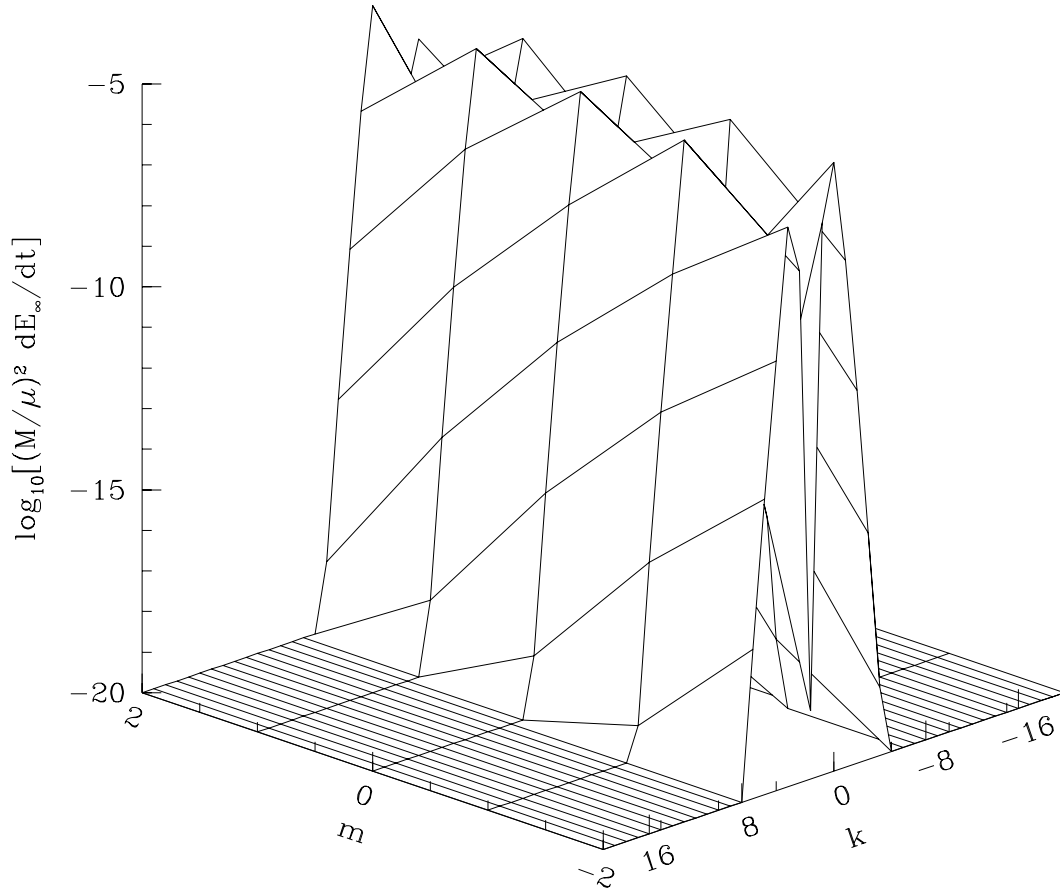


FIG. 7. The spectrum of energy for  $l = 2$  modes radiated to infinity by orbits with  $r = 7M$ ,  $\iota = 60.14^\circ$  about a black hole with  $a = 0.05M$ . The distribution is fairly narrow with respect to  $k$ , particularly when compared with the distribution for  $a = 0.95M$  (Fig. 4). This is because the Teukolsky potential is not very transmissive to high-frequency modes for small  $a$ . Note, though, that the distribution shows the potential is more transmissive to corotating modes ( $m\omega > 0$ ) than to counterrotating modes, just as in the case of large  $a$ .



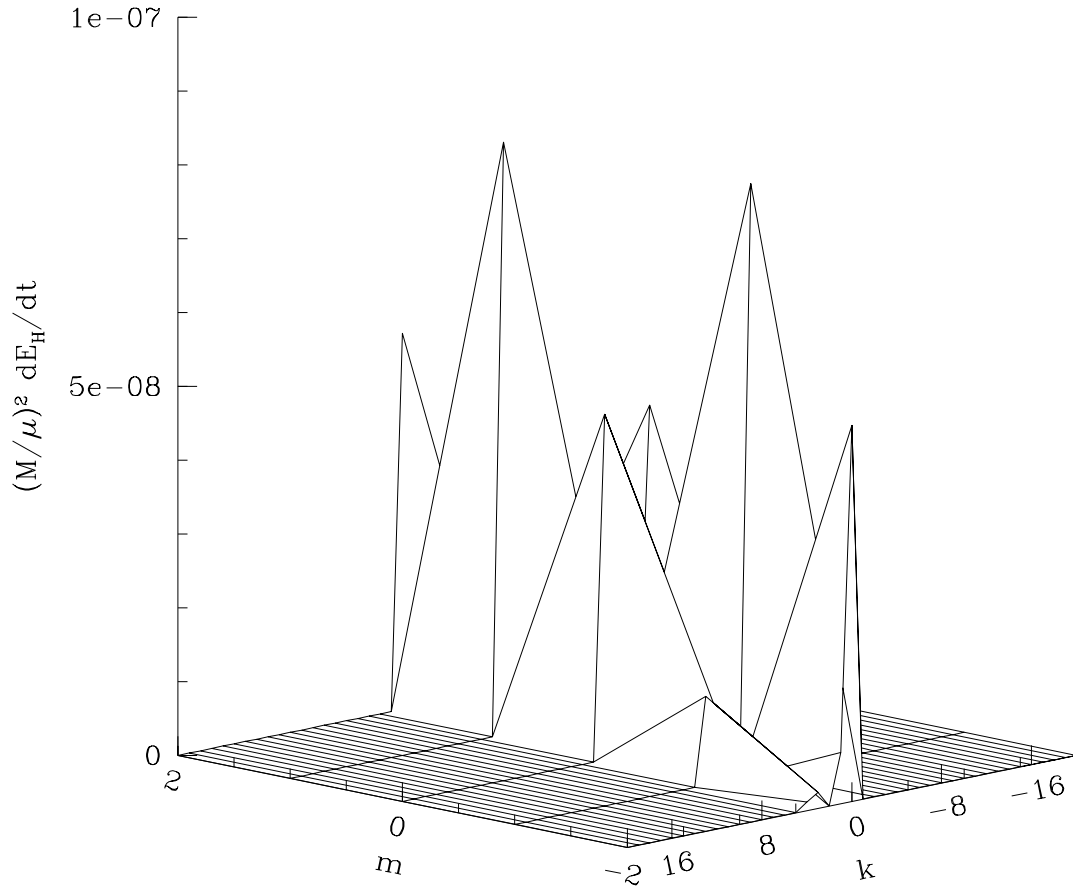


FIG. 8. The spectrum of energy radiated down the event horizon for  $l = 2$  modes for orbits with  $r = 7M$ ,  $\iota = 60.14^\circ$  about a black hole with  $a = 0.05M$ . In this case, the distribution is nowhere negative: the ergosphere for such a slowly rotating hole is practically irrelevant, and as a consequence we never see any superradiant scattering.

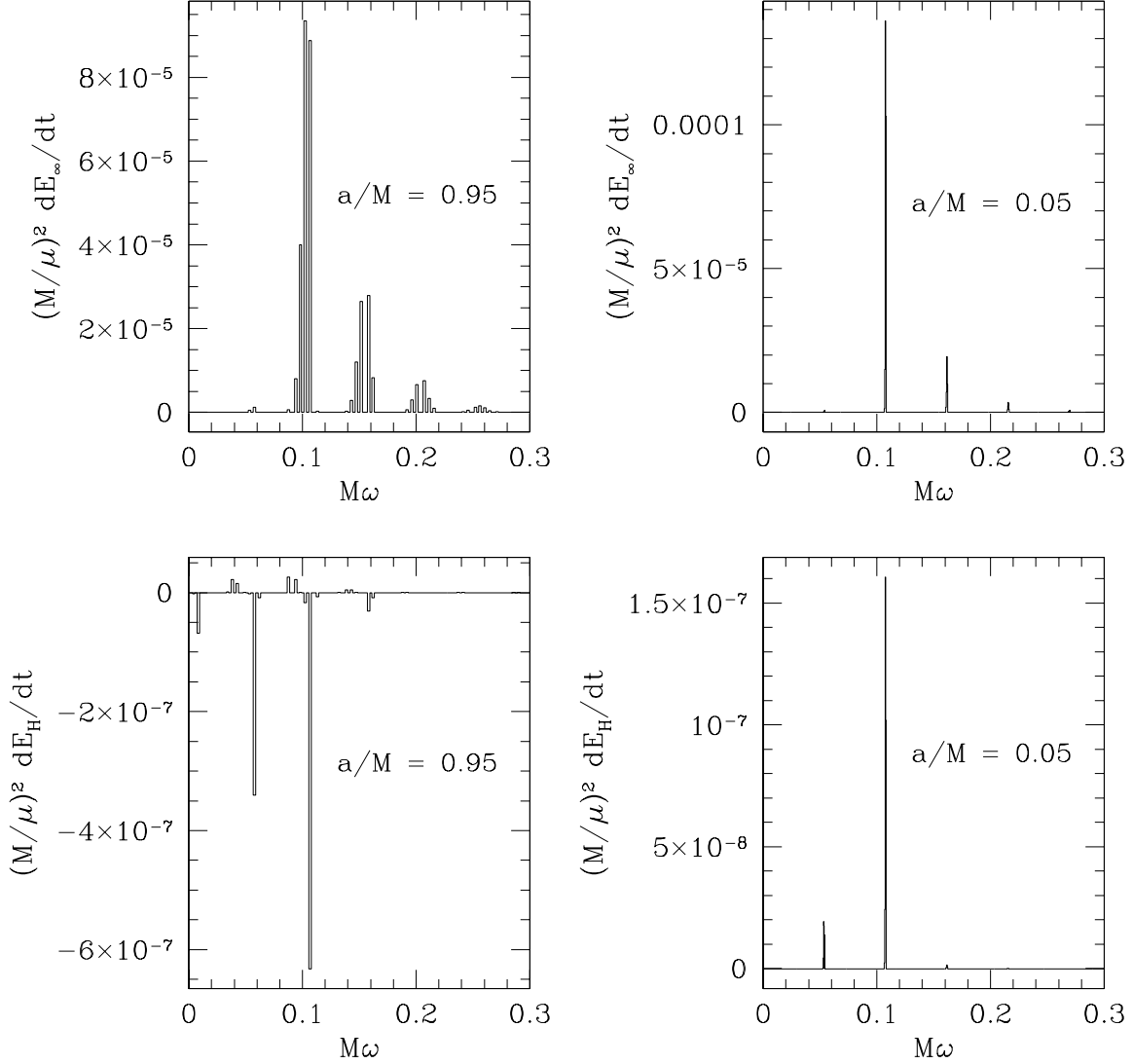


FIG. 9. Energy spectra  $dE/dt$  as a function of frequency  $\omega$  for orbits at  $r = 7M$ . The spectra on the left are for  $a = 0.95M$ ,  $\iota = 62.43^\circ$ ; the spectra on the right are for  $a = 0.05M$ ,  $\iota = 60.14^\circ$ . The top two spectra are  $dE_\infty/dt$ , the energy radiated to infinity; the bottom two are  $dE_H/dt$ , the energy down the horizon. All spectra have been summed over  $l$ . In all cases, the greatest amount of radiation comes out at  $\omega \sim 0.1/M$ ; this corresponds to  $\omega \sim 2\Omega_\phi \sim 2\Omega_\theta$ . For  $a = 0.95M$ , the power is smeared over several frequency bins near each peak. By contrast, the power is well-confined near a single bin for  $a = 0.05M$ . In both cases, there is significant power at several sum and difference harmonics of  $\Omega_\phi$  and  $\Omega_\theta$ . For  $a = 0.95M$ , these frequencies are different enough (relative difference  $\sim 10\%$ ) that the effect of these harmonics is quite marked. For  $a = 0.05M$ , the frequencies are practically identical (relative difference  $\sim 0.5\%$ ), so the harmonics are barely distinguishable from the main peak.

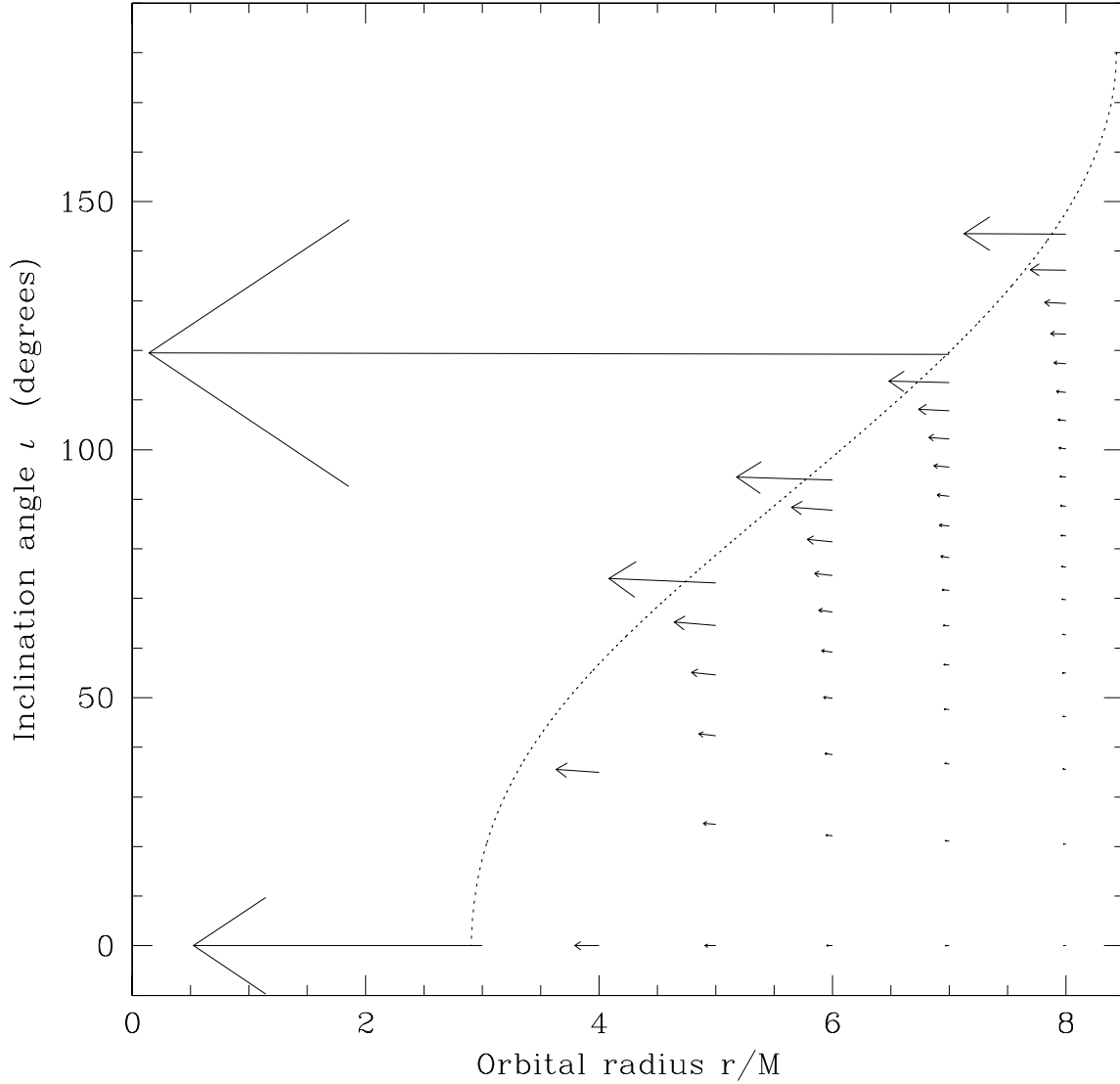


FIG. 10. The effect of radiation reaction on orbits around a black hole with  $a = 0.8M$ . The dotted line is the maximum allowed inclination angle; orbits tilted beyond that line are dynamically unstable and rapidly plunge into the black hole. Each arrow is proportional to the vector  $[(M/\mu)\dot{r}, (M^2/\mu)\dot{i}]$ . Thus, the orientation of the arrow indicates the direction in phase space to which radiation reaction drives the orbit; the length of the vector indicates how strongly it is so driven. In all cases, the vectors point inwards and upwards — radiation reaction drives circular orbits to smaller radii and larger inclination angles (except when  $\iota = 0^\circ$  or  $180^\circ$ , in which case the inclination angle does not change). The rate at which the inclination angle changes is rather slow, especially compared to the rate at which the radius changes. Note the very long vector (indicating extremely rapid orbital evolution) at  $\iota \simeq 120^\circ$ ,  $r = 7M$ . This orbit evolves so quickly because it happens to lie extremely close to the maximum allowed angle — it is barely dynamically stable, so a small push from radiation reaction has marked effects.

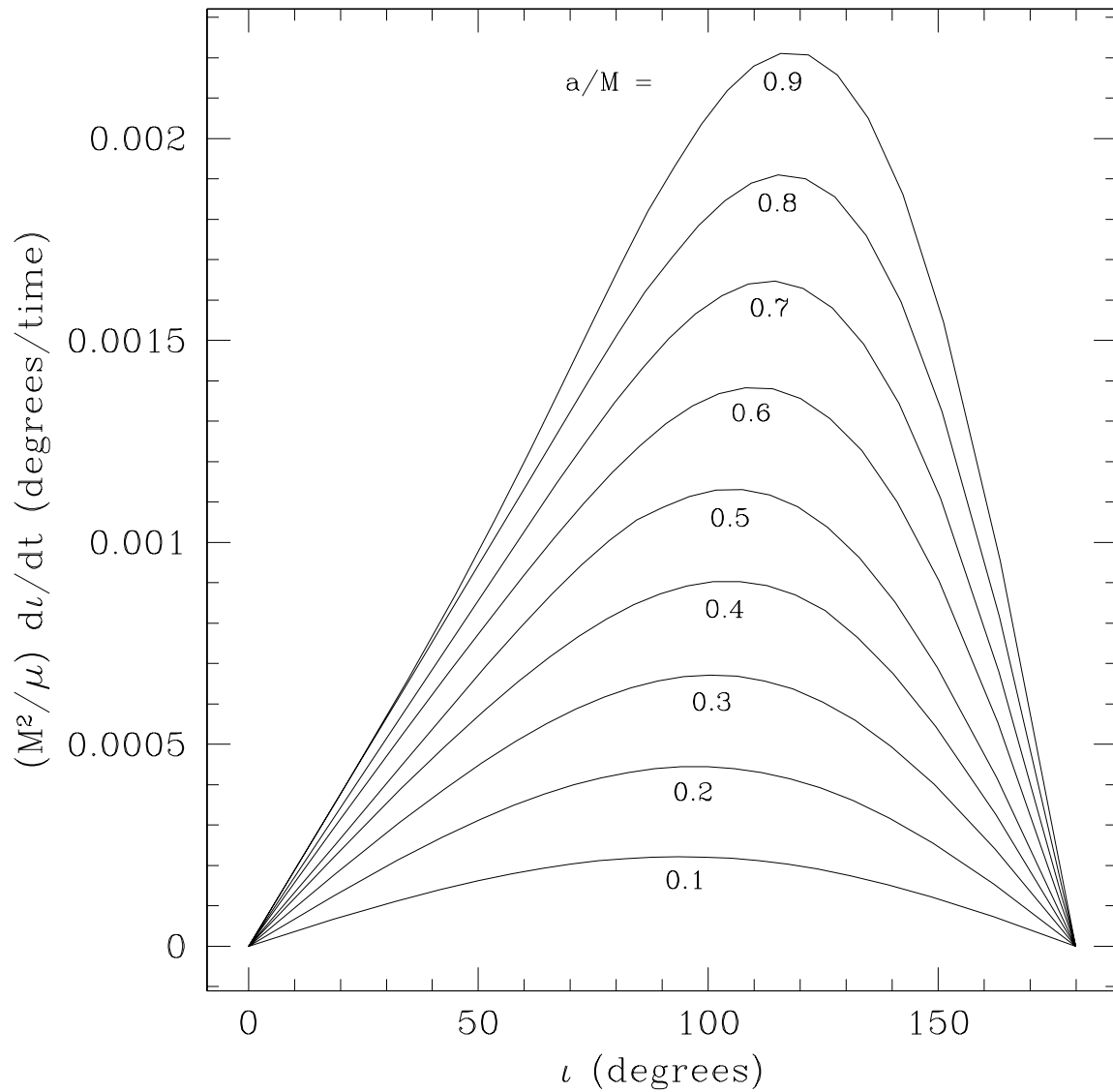


FIG. 11. The rate of change of the inclination angle  $i$  versus  $\iota$ , parameterized by black hole spin. All curves are for orbits at  $r = 10M$ . For large spin, the maximum rate of change of the angle occurs for  $\iota > 90^\circ$ , in contrast to the post-Newtonian prediction, which yields  $i \propto \sin \iota$  [cf. Eq. (3.9)].